Universidade do Porto

Faculdade de Engenharia da Universidade do Porto

Instituto de Ciências Biomédicas Abel Salazar

Instituto de Engenharia Biomédica

High-throughput development and analysis of prevascularized spheroids for therapeutic cell delivery

Daniel José Teixeira Oliveira Carvalho

Masters in Bioengineering – Molecular Biotechnology

Porto, September 2016

High-throughput development and analysis of prevascularized spheroids for therapeutic cell delivery

Daniel José Teixeira Oliveira Carvalho

Thesis for Masters in Bioengineering

FEUP – Faculdade de Engenharia da Universidade do Porto

ICBAS – Instituto de Ciências Biomédicas Abel Salazar

Supervisor:

Cristina Barrias, Ph.D. **i3S/INEB**

Co-supervisor:

Tália Figueiredo, Ph.D. **i3S/INEB**

i3S – Instituto de Investigação e Inovação em Saúde

INEB – Instituto de Engenharia Biomédica, Universidade do Porto

Abstract

Stem cell therapies (CT) are likely to play a vital role in the next generation of healthcare, owing to their potential of providing novel treatments for currently unmet human diseases and injuries. Yet, several clinical trials with CT, which have largely explored the use of mesenchymal stem cells (MSC), have consistently reported rather modest and transient therapeutic outcomes. Indeed, when single-cell suspensions are administered into a patient, cell loss and death often occur shortly after transplantation, ultimately leading to compromised cell function and engraftment. Thus, translating CT into medical practice will largely depend on the development of more efficient cell stem delivery formats. Several preclinical studies have demonstrated that the use of cells pre-assembled as aggregates, often referred as spheroids, might enhance therapeutic efficiency over single cells, namely by improving retention and survival in host tissues. Stem cells spheroids containing also endothelial cells (EC) have recently showed promise, as they might accelerate vascular integration with the host, a key feature for cell survival. Yet, prevascularized spheroids described so far have often been generated using platforms difficult to scale-up, have mostly used mature EC, which present lower clinical relevance than EC progenitors (EPC), and have often been poorly characterized.

In this context, the present study aimed at (1) establishing a methodology for high throughput (HT) production and analysis of prevascularized spheroids of MSC combined with EPC, and at (2) characterizing the organization and function of these cells within the established three-dimensional (3D) cellular microenvironments, particularly regarding extracellular matrix (ECM) deposition and formation of vascular-like microstructures. Late EPC, also called outgrowth endothelial cells (OEC), were combined with MSC at a 1:1 cell ratio and cocultured for up to 21 days in nonadhesive microwell arrays casted from commercially available precision molds. Each microwell arrays enabled the generation of 81 spheroids, which could be directly processed and analysed *in situ* using a protocol designed and optimized herein, that ultimately allowed histological and immunohistochemical analysis of several spheroids per section. Within 24h, OEC in presence of MSC were able to form compact spheroids, which remained active for up to 21 days. These spheroids accumulated abundant amounts of ECM proteins such as fibronectin (FN) and collagen type IV. Interestingly, in MSC-OEC spheroids,

FN fibers polarized at the periphery, whereas in MSC monoculture spheroids, used as controls, FN was distributed throughout the whole spheroid, suggesting that OEC in coculture spheroids established a bidirectional crosstalk with MSC, modulating the dynamic re-arrangement of the 3D microenvironment. OEC were found to assemble into two specific vascular microstructures, namely as aligned cells at the periphery and as clusters at the core, sometimes presenting some EC sprouting. The angiogenic potential of these vascular-like microstructures, at different culture times, should be further assessed in future studies, both *in vitro* and *in vivo*.

In summary, this study shaded some light on the behavior of clinically relevant OEC, when pre-assembled as spheroids. In particular, it showed that a HT platform could be used to generate/analyze uniform coculture spheroids containing OEC that presented some potentially relevant features for CT, such as maintenance of high integrity over long periods of culture, expression of abundant ECM amounts and some level of vascular organization. As such, results from this study provided meaningful insights that may contribute for future developments in spheroid-based CT.

Sumário

As terapias de células estaminais (CT) poderão vir a desempenhar um papel vital na próxima geração de cuidados de saúde, devido ao seu potencial terapêutico para patologias actualmente sem cura. No entanto, vários ensaios clínicos envolvendo as CT, que têm vindo a explorar sobretudo o uso de células estaminais mesenquimais (MSC), têm consistentemente reportado eficiências terapêuticas modestas e transitórias. De facto, quando suspensões de células são administradas a um paciente, ocorre perda e morte celular em pouco tempo após transplantação, comprometendo assim a funcionalidade e integração celular. Desta forma, a translação das CT para a prática clínica dependerá, essencialmente, do desenvolvimento de veículos de entrega de células estaminais mais eficientes. Vários estudos pré-clínicos têm demonstrado que a utilização de células pré-organizadas em agregados, geralmente designado por esferóides, pode melhorar a eficiência terapêutica em comparação com células em suspensão, visto que podem melhorar a retenção e a sobrevivência celular nos tecidos do hospedeiro. Esferóides contendo células endoteliais (EC) no seu interior têm vindo a demonstrar um potencial crescente para as CT, visto que podem acelerar a integração das células dadoras com o sistema vascular hospedeiro, uma característica essencial para a sobrevivência celular. No entanto, os esferóides pré-vascularizados descritos até à data têm sido muitas vezes produzidos usando plataformas que não permitem a sua produção em larga escala, têm usado na maioria das vezes EC maduras, que apresentam uma relevância clínica inferior às EC progenitoras (EPC), e têm sido frequentemente caracterizados de forma pouco exaustiva.

Neste contexto, os objectivos do presente estudo foram: (1) estabelecer uma metodologia para a produção e análise em larga escala (HT) de esferóides pré-vascularizados de MSC combinados com EPC; e (2) caracterizar a organização e função destas células dentro dos microambientes celulares tridimensionais (3D) estabelecidos, nomeadamente em termos da deposição de matriz extracelular (ECM) e da formação de microestruturas vasculares. EPC tardias, também denominadas por *outgrowth endothelial cells* (OEC), foram misturadas com MSC numa proporção de 1: 1 e cultivadas até 21 dias em placas contendo *microarrays* produzidos a partir de moldes comercialmente disponíveis. Cada *microarray* permitiu a produção de 81 esferóides, que foram directamente processados e analisado *in situ* segundo

um protocolo idealizado e optimizado durante este trabalho, o qual permitiu a caracterização histológica e imunohistoquímica de vários esferóides por secção. Após 24 horas, as OEC na presença de MSC foram capazes de formar esferóides compactos, que permaneceram activos até 21 dias. Estes esferóides expressaram abundantemente fibras da ECM, como fibronectina (FN) e colagénio tipo IV. Curiosamente, nos esferóides MSC-OEC, as fibras de fibronectina polarizaram na periferia, enquanto que nos esferóides MSC, usados como controlos, as fibras de fibronectina distribuíram-se difusamente ao longo de todo o esferóide, sugerindo que as células OEC em esferóides de co-cultura estabeleceram uma comunicação bidireccional com as MSC, modelando a organização dinâmica do microambiente gerado ao longo da cultura. Neste estudo, as OEC foram capazes de se auto-organizar em dois tipos específicos de microestruturas vasculares, nomeadamente como células alinhadas à superfície e como agregados no interior dos esferóides, que por vezes apresentaram prolongamentos endoteliais. O estudo do potencial angiogénico destas estruturas, a diferentes tempos de cultura, deveria ser mais aprofundado, quer *in vitro* como *in vivo*.

Resumindo, o presente estudo desvendou alguns aspectos do comportamento de EC clinicamente relevantes, quando organizadas em esferóides. Em particular, mostrou-se que a plataforma HT aqui descrita pode ser usada para produzir e analisar esferóides uniformes em grande escala. As OEC demonstraram possuir algumas características interessantes para CT, como por exemplo, a manutenção da integridade do esferóide ao longo de extensos períodos de cultura, a expressão abundante de matriz extracelular e a capacidade para formar estruturas vasculares. Desta forma, os resultados deste estudo forneceram novas pistas que poderão contribuir para futuros desenvolvimentos ao nível das CT.

Acknowledgments

To my supervisor, Dr. Cristina Barrias, I would like to express my deepest gratitude for the opportunity that was given to me and her constant support throughout my thesis.

My sincere appreciation is extended to Ewa Bauman. It was a pleasure to work with her, side by side.

I would like to thank to Ana Luísa for all the help that was given to me, as well as to Pedro Granja's team members: Filipa Sousa, Tiago dos Santos, Daniel Ferreira, Juliana Dias, Manuela Brás, Rúben Pereira, Sara Neves, Carlos Diogo, Luís Tavares, Manuel de Barros, Mariana Neves, Miguel Ferreira and Adele Cook.

A special thanks to the members of Achilles team, Miguel Ferreira, Elsa Silva and Raquel Almeida for the long nights spent together writing our last words in Leiden (sorry for the window, folks).

I want to thank my family, particularly my mother and father for supporting and giving me all the conditions that I needed to study in the university. My gratitude is extended to my grandmother, uncle, sister and, of course, my beloved dog. Also to my deceased grandfather, who would be more than proud.

I would like to express my deepest gratitude to my previous high school science teachers, particularly professor Helena Valente. Among different aspects, her passion for science strongly fascinated me to pursue a scientific career. I will always thank her for that.

And finally to Tália Figueiredo, my "mini-boss", for always being there when I needed and teaching me how to be a good scientist.

Table of Contents

List of Figures

List of Tables

List of Abbreviations

2D	Two-dimensional
3D	Three-dimensional
APES	(3-aminopropyl)triethoxysilane
aPKC	atypical protein kinase C
BSA	Bovine serum albumin
CT	Stem cell therapies
DAH	Differential adhesion hypothesis
DAPI	4',6-diamidino-2-phenylindole
DMEM	Dulbecco's Modified Eagle Medium
EC	Endothelial cells
ECM	Extracellular matrix
EGM-2MV	Microvascular Endothelial Cell Growth Medium
EPC	Endothelial progenitor cells
EtOH	Ethanol
EX/EM	Excitation/Emission
FBS	Fetal bovine serum
FN	Fibronectin
HAF	Human aortic fibroblasts
H&E	Hematoxylin & Eosin
HDMEC	Human dermal microvascular endothelial cells
HSCT	Human hematopoietic stem cell transplant
HT	High-throughput
HUASMC	Human artery smooth muscle cells
HUVEC	Human umbilical vein endothelial cells
MSC	Mesenchymal stem cells
OB	Osteoblasts
OEC	Outgrowth endothelial cells
ON	Overnight
PBS	Phosphate buffer saline
PDGF-ß	Platelet-derived growth factor ß
PDMS	Poly(dimethylsiloxane)
PEG	Poly(ethylene glycol)
PFA	Paraformaldehyde
pHEMA	Poly(2-hydroxyethyl methacrylate)
PI	Propidium Iodide
P/S	Penicillin/streptomycin
PVA	Poly(vinyl alcohol)
RT	Room temperature
ULA	Ultra-low attachment
w/o	Water-in-oil
ZO-1	Tight junction protein 1

Chapter I

Introduction

I.1. Stem cell therapies

The pharmaceutical industry has long been dominated by the use of small molecule and protein drugs as therapeutic agents (natural and synthetic molecules, recombinant hormones, antibody-based drugs, among others). Pharmaceutical drugs have proved remarkable outcomes in restoring health and prolonging life span, but in the twenty-first century, an increasing number of human diseases and injuries are unlikely to be treated by drugs alone[1]. Over the past decades, the use of cells has emerged as a next-generation therapy to meet critical patient needs[2,3]. Indeed, CT aim to restore damaged or diseased tissues by using living cells as therapeutic entities. In principle, cells have attributes that extend beyond those of molecular drugs. For instance, cells can adapt, migrate and execute complex biological upon recognition of their target in a spatial and temporal controlled manner[2,4]. This allows them to be better suited to address acute and chronic diseases that require precise control over distribution and therapeutic action[2].

Since the first human hematopoietic stem cell transplant (HSCT), which is now a routine clinical practice for hematologic malignancies and congenital or acquired bone marrow failure[5], and undoubtedly the most successful stem cell therapy to date, CT have successfully addressed a wide range of unmet human diseases[6,7]. Between 1988 and 2010, the number of CT-approved products has reached 675 000 units, being used by more than 300 000 patients worldwide[7]. Additionally, an ever-increasing number of CT schemes are currently under clinical trials. According to a 2014 study[4], a total of 1342 active clinical trials are being conducted worldwide, where, excluding the use of hematopoietic cells for HSCT, MSC appear as the most reported cell type (28%). The same study reported that the main targets of CT are oncological disorders, representing almost half of total CT clinical trials identified, followed by cardiovascular diseases (6%), including acute coronary syndrome, congestive heart failure, and refractory angina; and immunological disorders, such as graft vs host disease, Crohn's disease and immunodeficiency[4].

I.2. Current challenges

Apart from HSCT, dermal and corneal applications, while CT preclinical and clinical trials have been shown promise and continue to grow both in number and in the variety of cell types studied, their translation into commercial efficient treatments is far from expected and hampered by numerous technical, safety, legislative and ethical struggles[8]. Moreover, clinical trials have consistently showed modest therapeutic efficiency, in part owing to the very low rate of long-term cell engraftment. Indeed, several preclinical studies and clinical trials reported that, when single-cell suspensions are administered into a host, in general, more than 90% of injected cells are lost in the following days[9–12] and only less than 7% of donor cells managed to integrate into host system[11,13,14].

As reported, for example, in several studies in the field of heart repair[15], cell engraftment efficiency is low due to a significant washing out of implanted cells from the target site at the time of injection or during early engraftment. This leakage not only decreases the amount of cells at the retention site, but also leads to unwanted systemic dissemination, which may raise further safety concerns[16]. Additionally, cells that were able to be retained at the lesion site may suffer from adverse microenvironmental conditions, including ischemia, caused by insufficient vascularization, and local inflammation that often results in cell death. Furthermore, cells, particularly anchorage-dependent ones, may enter in programmed cell death due to the lack of attachment posttransplantation[17], in a process called anoikis (from Greek: "without home"[18]). Taking into consideration that transplanted cells can exert a healing outcome by secreting soluble factors (chemokines, cytokines and growth factors) at retention site (paracrine mechanisms) and/or by directly replacing diseased cells (structural mechanisms), the extent of donor cell loss upon transplantation highly determines the therapeutic potential of CT[16].

Considering the numerous challenges mentioned above, whether CT will manage to spread into the marketplace as a medical practice strongly depends on cellular enhancement and/or on the development of more efficient cell-delivery formats. At this stage, it is required both a deeper understanding of stem cell biology and the therapeutic mechanisms exerted by donor cells; and the establishment of cellular and tissue engineering as foundation sciences for advanced CT[1,2]. Alike to what happened in the earlies of pharmaceutical industry, in which therapeutic limitations of the first commercialized drugs were overcome by the contribution of protein engineering and synthetic organic chemistry, cellular and tissue engineering are

thought to play a paramount role in moving forward currently CT[1,2]. In fact, different strategies of cellular enhancement have been recently reported to boost cell engraftment in the host system, including genetic manipulation and preconditioning cells before transplantation (reviewed elsewhere[19]). Genetically modified MSC have consistently been reported and showed to better improve cardiac function and to reduce infarct size, in comparison with non-modified MSC treated animal models[20-22]. Some of the most successful genetic approaches include the transduction of genes encoding antiapoptotic factors like bcl2[20] and Akt[22] or overexpression of transcription factors, growth factors, chemokines and proangiogenic factors[21]. Similarly, preconditioning cells through heat shock or incubation with pharmacological agents before transplantation have shown to enhance cell survival at the myocardial infarct site[20]. Based on tissue engineering strategies, the use of biomaterial-based carriers to protect transplanted cells from harsh *in vivo* conditions has also shown benefits[23-25] and is becoming more common in the clinics[23].

I.3. Multicellular spheroids for augmented CT

Recently, the use of cells pre-assembled into multicellular aggregates, often referred as microtissues, has emerged as a promising alternative to single-cell injection. Different approaches to create multicellular constructs for CT are under investigation, including biomaterial-based strategies, where cells are cultured on-top or within 3D scaffolds, and scaffold-free approaches such as cell sheets or 3D aggregates (the so-called spheroids). Among these models, spheroids have been recently gathering increasing interest among the scientific community[26]. Indeed, spheroid cultures are currently being explored for several biomedical applications, including CT for tissue regeneration[27-31], drug screening[27] and 3D cell culture models that more closely mirror their *in vivo* counterparts[32]. Spheroids can be defined as 3D cellular aggregates that preserve cell-cell and cell-matrix interactions, where cells are able to engage tissue-specific functions.

Several reports have been suggesting that pre-assembling donor cells as spheroids can increase therapeutic efficiency for a variety of diseases and injuries, including cartilage damaged[33], neuronal diseases such as Parkinson's[34], myocardium infarction[35], hindlimb ischemia[36] and traumatized dental pulp[31]. When compared to monodisperse cells, spheroid cultures have shown to (1) secrete higher amounts of proangiogenic, antiapoptotic and anti-inflammatory factors[28,37-39]; (2) produce endogenous ECM[40], which in turn makes implanted cells more easily retained at the target site and less susceptible to anoikis; and to (3) be better

protected against adverse conditions such as hypoxia and oxidative stress[39,41,42]. These features ultimately lead to higher cell survival and engraftment[43,44].

Despite spheroid culture apparent advantages in comparison to single-cell delivery, its widely adoption as a cell-delivery format for CT has not been as fast as expected[26]. Indeed, the mechanisms underlying spheroid formation and stem cell behavior within spheroid micromilieu are not yet fully understood, which in turn may mitigate its use. Additionally, spheroid cultures, as well as other 3D cultures, have long been considered as expensive, complex of use and non-reproducible systems. As any other regenerative medical application, CT requires reproducible and scalable products. As so, the global acceptance of spheroids also depends on the development of platforms that enable production of high amounts of uniform spheroids and compatible with standard biochemical analysis, the ones traditionally used in two-dimensional (2D) cultures, and with HT screening assays.

Therefore, herein, a comprehensive focus is provided to the mechanisms underlying the formation of spheroids as well as a description of recent advances in the HT platforms that enable scalable generation of spheroids.

I.4. Generation of spheroids

When seeded under nonadhesive culture conditions, anchorage-dependent cells may spontaneously aggregate (i.e. self-aggregation) into a compact tissue-like spheroid capable of engaging similar functions to its *in vivo* counterparts. However, in biological systems, natural tissues may represent more complex structures with a specific spatial distribution of multiple cell types. During embryonic development and regeneration, tissue morphogenesis relies on cell sorting events, in which an initially disordered cluster of cells spontaneously segregate into distinct tissue-specific cell compartments[45]. These cell sorting mechanisms can also be recapitulated in spheroid cultures, when at least two different cell types are cultured together.

I.4.1. Cell assembly into monoculture spheroids

When cells are cultured on nonadhesive substrates or in suspension, intercellular adhesions prevail over cell-substrate interactions. According to the differential adhesion hypothesis (DAH) formulated by Steinberg in 1962[46], under such culture conditions, monodispersed cells tend to minimize the surface free energy by maximizing intercellular interactions, spontaneously aggregating into a more thermodynamically-stable spherical cluster (**Fig.1**). Nevertheless, non-spherical geometries, including rods, tori and lumen-containing

4

honeycombs can be obtained, for example by culturing cells on nonadherent micromolds with different topographies[47,48]. After aggregation, spheroids generally decrease in size due to strong cell-cell interactions, ultimately forming a compact tissue-like construct [49] (**Fig.1**).
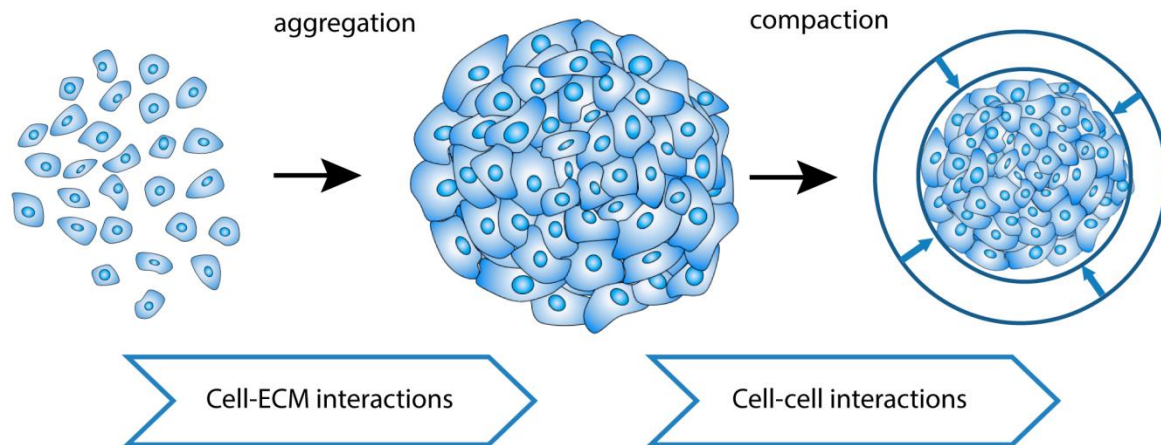

Figure 1 - Mechanisms underlying spheroid formation in monocultures. Monodispersed cells with high surface tension self-aggregate into a tissue-like cluster. According to Lin *et al.*[49] this self-aggregation step is primarily mediated by integrin-matrix adhesions. Then, spheroids decrease in size due to strong cell-cell interactions, mainly driven by cadherin-mediated adhesions, ultimately forming compact spheroids. It should be noted that this study was performed using specific cell types and so, these mechanisms may vary for other cell types.

Several studies have showed that the forces driving cell aggregation largely depend on intercellular adhesions mediated by cadherins, a superfamily of homophilic adhesion Ca^{2+}-dependent glycoproteins. Duguay *et al.*[50] reported that, contrarily to cadherin-expressing mouse fibroblasts, cells with inhibited cadherin expression failed to form compact spheroids. Similarly, Shimazui *et al.*[51] showed that spheroid formation by renal cell carcinoma cell lines was inhibited by antibodies against E-cadherin, demonstrating its paramount role.

Although cell-cell adhesions have long been considered the primary mediator of tissue cohesivity, several studies have demonstrated that integrin-ECM adhesion can also contribute for microtissue cohesivity by indirectly linking adjacent cells together[52], especially for cells that rapidly secrete ECM components, such as ovarian cells[53], hepatoma cells[49], carcinoma cells and fibroblasts[54]. Using tissue surface tensiometry, Robinson *et al.*[52] measured a strong cohesivity in $\alpha_v\beta1$ integrin-transfected cell-derived microtissues that was independent of cadherin expression and significantly stronger than N-cadherin-transfected cells. Other studies demonstrated that fibroblasts lacking fibronectin expression were unable to assemble

into compact spheroids. Consistently, Lin *et al.*[49] showed that, from different E-cadherin-expressing hepatoma cell lines, only the one with low ECM secretion was unable to form spheroids. Moreover, integrin-blocking agents partially delayed initial cell aggregation, while inhibiting E-cadherin activity did not prevent aggregation, but inhibited spheroid compaction. In light of these results, Lin *et al.*[49] proposed a model of spheroid formation, in which secreted ECM components act as anchors for initially attachment of monodispersed cells via integrins, forming loose aggregates. Then, as cells coalesce, strong cadherin-mediated cell-cell interactions take place, ultimately forming compact spheroids (**Fig. 1**).

Although more results should be obtained to support this theory, one can accept that depending largely on the cell type, the mechanisms underlying spheroid dynamics are driven by cell-cell adhesions as well as by indirect binding through integrin-ECM interactions.

I.4.2. Cell assembly into coculture spheroids

As in gastrulation and organogenesis, intercellular adhesions mediated by cadherins are considered to be a major determinant of tissue boundary formation in spheroid cultures[55]. In coculture spheroids, several studies demonstrated that the cell type expressing cadherin at lower level envelops cells with higher cadherin expression levels, forming concentric spheroids[45,47,50,56,57] (**Fig.2**). On the other hand, when cadherin expression levels of both cell types are similar, cells tend to form randomly mixed spheroids[50]. According to the DAH, these cell sorting events are driven by differential intercellular surface tensions originated from cell-cell and cell-ECM interactions, operating in the same manner as interfacial tensions do in the rearrangements of immiscible liquids[56]. As oil with lower surface tension spreads over a single droplet of water, cells with lower surface tension (i.e. lower cohesive adhesions) coalesce and spread over any other cells with higher surface tension, in order to minimize the total surface free energy. Apart from cadherins, other cell-cell adhesion molecules have been demonstrated to guide cell sorting as hypothesized by the DAH. For example, Bao *et al.*[58] reported the formation of concentric spheroids, in which cells expressing connexin, a family protein that assemble into gap junctions, segregated into the inner core, while connexin-negative cells migrated to the periphery.

It should be noted that the DAH is one of the many other hypothesis and factors dictating the dynamic and complex cell patterning in coculture spheroids. This topic is further detailed in section I.6.
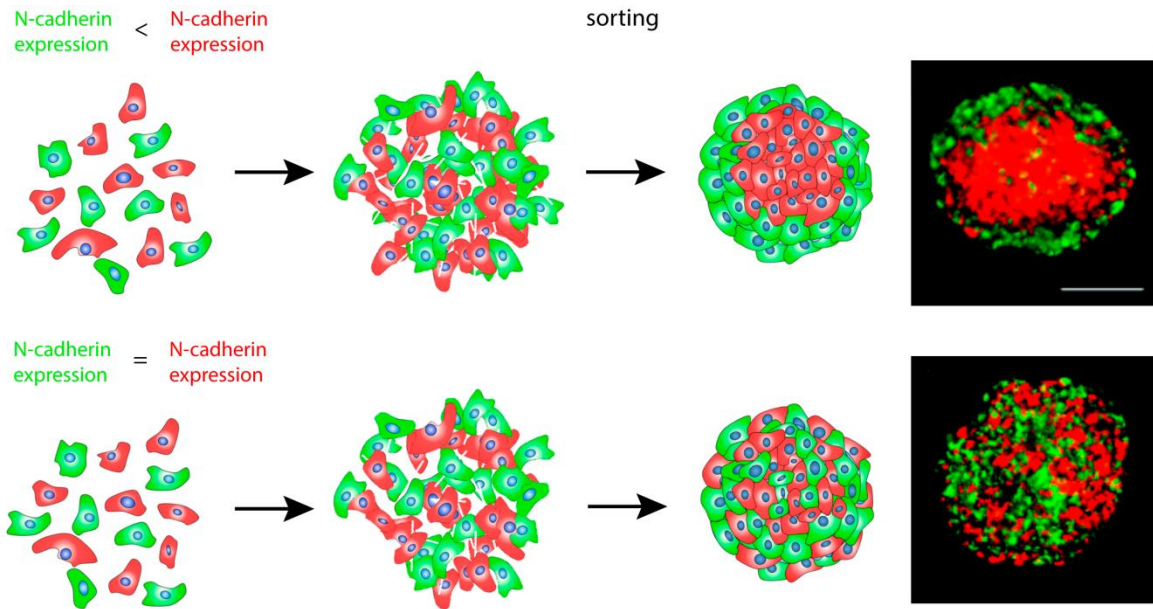
Figure 2 – DAH in cocultured spheroids. According to the DAH, in a monodisperse mixture of two epithelial different cell types with different expression levels of N-cadherin, cells with the higher expression levels (red cells) segregate into the inner core of the microtissue, while the cells with lower expression levels (green cells) migrate into the periphery. On the other hand, when the expression levels are equalized, an intermixed microtissue is formed, demonstrating the paramount role of N-cadherins for sorting mechanisms in coculture spheroids. Fluorescence images retrieved from[56]. Scale bar 100 μm.

I.5. Enabling platforms for scalable spheroid production

Various techniques have been developed to enable spheroid formation. These include (1) pellet cultures[59]; cultivation in (2) gyratory shakers, roller bottles and spinner flasks[60,61]; (3) microgravity modulators[62,63]; and in (4) non-adhesive culture vessels[64,65]; (5) hanging-drop cultures[66]; (6) cell sheets[67]; (7) magnetic levitation[68]; (8) droplet microfluidics[69] and the recently proposed (9) floating liquid marble technique[70]. While most of these methods have been well described elsewhere[27,71,72], herein a comprehensive focus is given to technologies that enable the production of uniform-sized spheroids at large and reproducible scale, making it transposable for widely commercial adoption.

Although commercially available gyratory and spinner flasks are able to produce large amounts of spheroids, these are often heterogeneous in size and shape[60,61]. Moreover, individual monitorization of spheroids and HT assays are still not compatible to date. Similarly, microgravity modulators, including the commercially available Rotating Wall Vessel bioreactor are still incompatible with real-time single-spheroid analysis and automated readout systems, despite the impressive progress in the production of physiologically-

relevant tissue constructs[62,63]. In fact, only few conventional methods such as non-adhesive plates and hanging-drop cultures have made significant advances in producing uniform-sized spheroids at larger scale. Moreover, recent advances in cell magnetic levitation and droplet microfluidics have greatly expanded their potential for monodisperse spheroid generation.
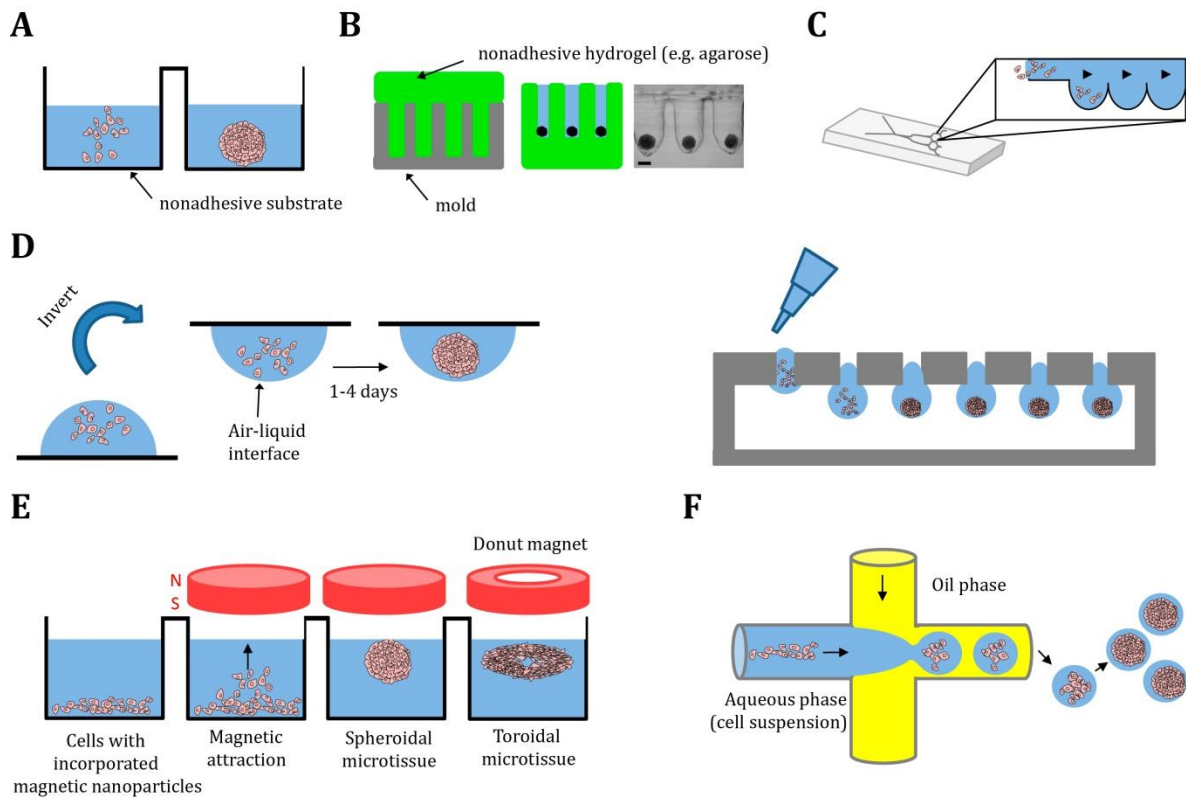
Figure 3- Platforms for spheroid generation at HT. (A-C) Nonadhesive-based methods; (D) The classical hanging drop technique is illustrated on the left side, while a design of a plate that allows higher throughput is represented in the right side; (E) In Cell Magnetic Levitation, cells are first incubated with the magnetic nanoparticles, and only then are seeded in nonadhesive wells to avoid premature cell aggregation. By applying a magnetic field, cells with nanoparticles incorporated will aggregate near the air-liquid interface. It is noteworthy that different shapes can be obtained by changing the magnet morphology; (F) Droplet microfluidics devices enable formation of microtissues within microcapsules by a necking process in the T-junction. These microcapsules in suspension can be then further analysed.

I.5.1. Liquid-overlay multiwell plates

The liquid overlay technique is a simple and widely used method for spheroid generation and long-term culture. As in conventional 2D cultures, monodispersed cells are simply seeded in a culture vessel, but contrarily, the vessel wall is made or coated with low cell adhesive polymers, such as agar[73], poly(2-hydroxyethyl methacrylate) (pHEMA)[74], agarose and

poly(ethylene glycol) (PEG)[64]. As such, cell attachment to the vessel wall is instead inhibited and cell-cell interactions are promoted, ultimately leading to spheroid formation on the culture vessel surface. Additionally, a centrifugation step or the use of U- or V-shape bottom wells may be helpful to further concentrate suspended cells at the bottom. When seeded on nonadhesive culture dishes, cells generally assemble into multiple heterogeneous spheroids.

However, when nonadhesive multiwell plates or microwells are used, it is possible to obtain one microtissue per well[64], where the size of the spheroids is primarily determined by the cell seeding density and microwell size (**Fig. 3A**). Many pre-coated plate-type products are commercially available for spheroid culture, which can be handled like traditional 2D culture plates, however generally commercialized at higher prices. Ultra-low attachment (ULA) pre-coated multiwell plates with concave-bottom wells, including the Nunclon Sphera™ Microplate, among others, enable the scale up in the generation of large numbers of monodisperse spheroids as well as easier monitorization and manipulation of individual spheroids, making this method compatible with HT approaches. In order to further scale up, multiwell plates such as the Aggrewell™ include an array of concave microwells at the bottom of each well, allowing for instance a 1200-fold increase in the production of uniform-sized spheroids (e.g. 9600 spheroids per Aggrewell™ 8-well plate), in which cell condensation is also promoted by the higher ratio between cell number and well size.

I.5.2. Nonadhesive micromolded hydrogels

Nonadhesive micromolded hydrogels have been used to form spheroids, in which the molten hydrogel solution is poured onto precision molds containing an array of the negative recesses (**Fig. 3B**). After gelation, the micromolded nonadhesive hydrogel is removed and placed into a standard culture dish, where it can be used as a nonadhesive culture vessel for spheroid formation and long-term culture[65]. Depending on the micromold design, complex spheroid shapes can be produced, such as rods, toroids or honeycombs[47]. More importantly, the micromolds can be autoclaved and then reused. One example of such system is the 3D Petri Dish® (Microtissues, Inc), a lab-made micro-molded agarose platform cast from commercially available precision molds. Apart from academic researchers, the 3D Petri Dish® has been adopted by pharmaceutical firms for cytotoxicity screenings and by cell-therapy companies[75]. Recently, primary postnatal cortical cells were seeded on the 3D Petri Dish® and formed electrically-active cortical microtissues with established synaptic connections, resembling

functional "mini-brains"[76]. The 3D Petri Dish® generated on the order of 1000 cortical microtissues per neonatal cortex tissue, demonstrating its potential for HT assays.

I.5.3. Microfluidic platforms

In order to add physiological-like fluid flow conditions, several microfluidic platforms have been recently developed for scalable microtissue generation, though its commercialization is still uncommon to date (reviewed elswhere[77]) (**Fig. 3C**). Generally, microfluidic systems for spheroid culture are designed based on microwells with concave geometries; higher cell number-well size ratios and/or nonadhesive polymers, including PEG, poly(vinyl alcohol) (PVA) and poly(dimethylsiloxane) PDMS, that together foster *in situ* cell aggregation[77]. These micro-platforms under controlled flow perfusion conditions have been extensively applied for drug screening and phenotypic spheroid studies using commercially available microplate readers and microscopes[78].

I.5.4. Hanging-drop technique

In classical hanging-drop methods (also known as gravity-enforced self-aggregation), droplets of single cell suspension (10-30μL) are pipetted onto a surface and then inverted upside down (**Fig. 3D-left**). By gravity, cells concentrate at the bottom of the hanging drop, at the air-liquid interface, forming a single spheroid per drop after 1-4 days, depending on the cell type[66]. Contrarily to nonadhesive methods, cells within hanging drops do not contact with a specific substrate, which could affect cell surface phenotype and behavior[71]. However, although it is relatively simple, conventional hanging-drop culture can be more labour-intensive and difficult to handle than nonadhesive methods. More importantly, since it is required to manually invert the plate, conventional hanging-drop technology is not adequate for massive production of spheroids.

To circumvent these problems, new hanging-drop plate designs have been developed such as the Perfecta3D® Hanging Drop Plate. This system from 3D Biomatrix is a hanging drop spheroid culture array plate with 384 access holes on the top of the plate. Small volumes of cell suspension are directly dispensed into the microscale holes, creating hanging drops that are stabilized by surface tensions (**Fig. 3D-right**). Using this system, it is possible to form 384 spheroids per batch without inverting steps, enabling the use of liquid handling robots to automatically pipette culture sites as well as plate readers for further HT colorimetric or fluorescence analysis[79,80].

I.5.5. Cell magnetic levitation

Recently, n3D Biosciences developed the commercially available Bio-Assembler™ Kit, which enables the formation of microtissues by magnetic levitation[68,81] (**Fig. 3E**). First, cells are magnetized by the uptake of magnetic nanoparticle-containing hydrogel fragments. Magnetized cells are then seeded onto a nonadhesive multiwell plate, where they are levitated and assembled near the air-liquid interface into a spheroid by a magnet located above the plate. Similarly, using the multiwell Bioprinting Kit, magnets are instead placed on the bottom of the multiwell plates, forcing suspended cells to form spheroids at the bottom (i.e. spheroid bioprinting)[82]. Over time, cells within the microtissue tend to spit out the nanoparticles, avoiding eventually long-term cytotoxicity effects[75]. Contrarily to other 3D technology offerings, magnetic levitation can take about 16h to form 3D multicellular constructs[83].

Using magnets of different geometries or different magnetic intensities along specific axes, it is possible to shape the 3D multicellular constructs to the desired configuration[68] (**Fig. 3E-right**). Additionally, microtissues can be magnetically manipulated, for example to create concentric multi-tissue models by sequentially assembling different magnetized cell types[82]. Overall, magnetic levitation, albeit quite expensive, is a versatile method for basic and complex experiments and can support HT assays for toxicity testing and drug development[84].

I.5.6. Droplet microfluidics

Droplet microfluidics is a miniaturized and HT emulsion-based technique to generate pico- to nanoliter-sized droplets by forcing two immiscible liquid phases to intersect at microchannel junctions (**Fig. 3F**). Recent advances in the field have expanded applications of microfluidics-generated droplets from encapsulated single-cell analysis to scalable microtissue generation[69,85,86]. In order to growth tissue constructs within each droplet, the cell suspension is normally injected into an aqueous inlet channel, which is forced to break into monodisperse droplets when intersected with the oil phase. The water-in-oil (w/o) droplets can be then cultured off-chip or stored in microchannel arrays and subsequently analysed by a wide variety of on-chip fluorescence and biochemical methods[86,87]. Recent studies reported the generation of more than 600 monodisperse droplets per minute, in which each droplet acted as a "microbioreactor" where encapsulated cells rapidly assembled into a size-controllable microtissue (2h-6h, depending on the cell type), due to the microscale confinement provided by the droplet, which encouraged cell-cell interactions[69,86]. Apart from the very HT generation

and storage of spheroids, droplet microfluidics enables a precise control over microtissue dimensions by tuning the droplet size and the cell density in the aqueous phase. These microfluidics devices can be purchased, albeit few companies are available, or alternatively fabricated in-house, using conventional soft lithography techniques.

I.6. Prevascularized spheroids

As previously mentioned, spheroids may exhibit several therapeutic advantages over single-cell delivery. However, spheroids for CT have been hampered by the limited or delayed vascularization of tissue substitutes upon transplantation[88–91]. Insufficient vascularization often leads to hypoxia and inadequate nutrient supply, ultimately inducing donor cell death and consequent decreased in function[89–91]. Thus, promoting *in vivo* neovascularization is currently a crucial need towards an augmented therapeutic outcome.

Pioneering studies have demonstrated that coculturing EC within spheroids *in vitro* (sometimes and hereinafter referred as prevascularization) can, in fact, promote integration with the host's vasculature and facilitate engraftment[92–94]. Indeed, several reports have shown that EC within coculture spheroids may assemble into vascular-like microstructures, which upon transplantation are able to anastomose with the host's vasculature[88,92,95], hence restablishing an adequate supply of oxygen and nutrients in the innermost parts of the tissue substitute.

Given these promising findings, a vast repertoire of prevascularized spheroids have been developed and successfully implanted for treating, among others, bone defects[95,96], dental pulp traumas[30,31] and heart diseases[93,97]. Studies have demonstrated that, depending on the culture conditions, EC may assemble into different types of vascular microstructures within coculture spheroids (**Fig.4**).
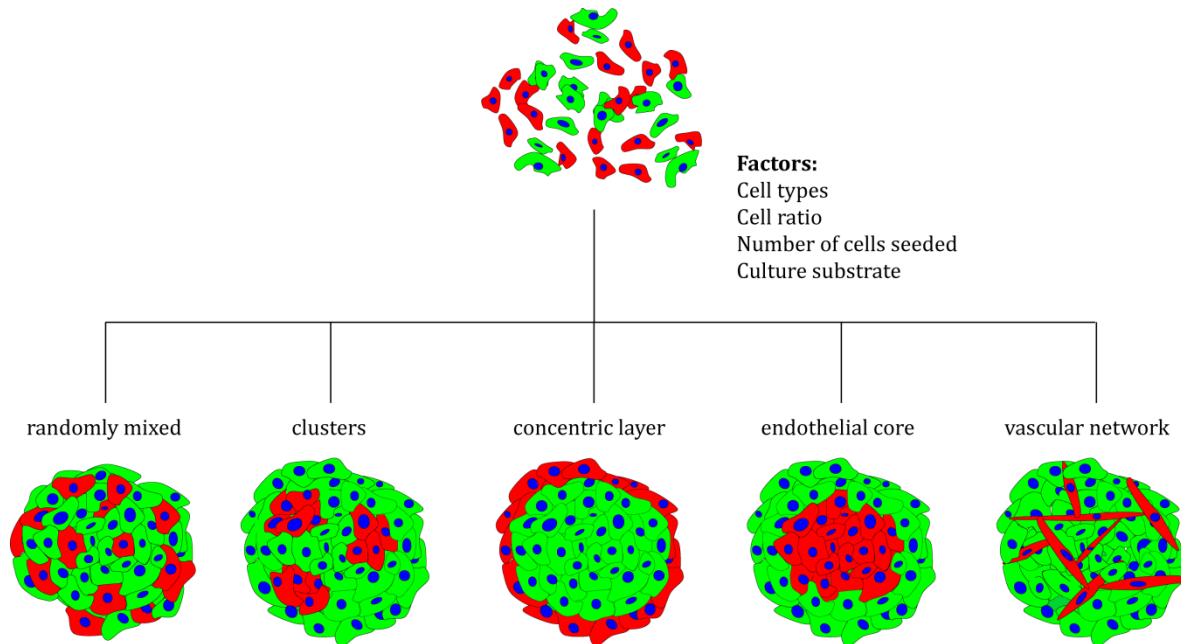
Figure 4 – Vascular patterning in coculture spheroids. Several types of vascular microstructures have been reported, including randomly mixed, clustered and concentric spheroids as well as endothelial cores and primitive vascular networks. The mechanisms by which EC (red) assemble into these vascular microstructures are complex and remain poorly understood. Nevertheless, recent findings have been suggesting that several biochemical and physical factors influence EC distribution within coculture spheroids such as cell types, ratio, the number of cells seeded, which will define spheroid size and consequently the mechanical forces throughout the spheroid, and the culture substrate where cells are seeded on.

In a pioneering study, Korff *et al.*[98] established a prevascularized spheroid system by combining equal amounts of human artery smooth muscle cells (HUASMC) and human umbilical vein EC (HUVEC) in liquid methylcellulose wells. Within 2 days, coculture spheroids spontaneously organized into a surface monolayer of EC, surrounding a core of HUASMC. EC at the surface were found to be less susceptible to apoptosis, showed downregulation of endogenous platelet-derived growth factor ß (PDGF-ß) expression and to have a higher number of interendothelial junctional complexes, in comparison to monoculture EC spheroids. Thus, and according to the authors, EC spontaneously segregated in a similar way to what is observed in physiological vessel walls, but in an inside-out orientation[98]. Additionally, EC in contact with HUASMC were found to acquire an EC *in vivo*-like mature phenotype that closely resembled quiescent vasculature[98]. A similar spatial distribution of EC in coculture spheroids was later observed in prevascularized spheroids with different cell types and ratios, such as 1:1 osteoblasts (OB):HUVEC[96]; 10:1 human aortic fibroblasts (HAF):HUVEC[28], and 2:1 hepatocellular carcinoma cell line: HUVEC[28]. However, Kelm *et al.*[28] demonstrated that, contrarily to what was previously reported by Korff and

colleagues[98], cocultured EC migrated into the innermost parts of 1:1 HUVEC-HUASMC spheroids. In this study, cells were assembled into spheroids without establishing any contact with a culture substrate as they were obtained by suspension in hanging-drops, rather than cultured in nonadhesive wells. As such, the authors suggested that the cell-culture substrate interactions might also contribute to the overall forces driving the organization of cells within coculture spheroids. This was further explored by Hsu *et al.*[29] by coculturing MSC and EPC on different substrates. Cells were able to assemble into coculture spheroids, but forming distinct patterns, including randomly mixed, clusters or concentric structures, depending on the substrates where they were cultured on[29]. Therefore, Hsu *et al.*[29] confirmed that, in fact, cell-substrate interactions influence cell distribution inside prevascularized spheroids. Furthermore, when seeded on the same substrates, but at different population ratios, cells assembled into distinct patterns inside coculture spheroids, hence indicating that the cell ratio also affects the final organization of prevascularized microstructures[29]. In order to assess the angiogenic potential of each cell pattern, cocultured spheroids, after 48h maturation on substrates, were further cultured on Matrigel and the formation of vascular networks was quantified after 8 days. Interestingly, the concentric spheroids revealed to have the strongest angiogenic potential among all the coculture spheroids. According to the authors, cellular patterns may in fact determine signal transduction, mediated for example by integrins and Notch ligands, and so, the signalling events of concentric spheroids may vary from those employed by other morphologies, which ultimately led to different angiogenic outcomes when transferred to Matrigel[29]. Nevertheless, further studies should be performed in order to elucidate the true role of distinct vascular microstructures on the angiogenic potential when implanted *in vivo*. Another interesting point of this study was the use of EPC. Although the majority of the research uses mature EC, particularly HUVEC as the EC source, EPC are clinically more relevant[99]. Over the past decades, EPC have been shown to directly contribute to neovessel genesis by being recruited and integrated into pre-existing vessels[100] as well as by forming *de novo* vascular vessels (i.e. vasculogenesis)[99]. However, the development of EPC-derived vascular structures in coculture spheroids remains largely unexplored.

Besides randomly mixed, localized clusters, endothelial cores and concentric spheroids, other studies demonstrated that other types of vascular cell arrangements can also be obtained in coculture spheroids, but strongly depending on an optimal cell ratio[95,101]. Kunz-Schughart *et al.*[101] were the first to report the formation of a capillary-like network of EC inside fibroblast-HUVEC spheroids for cell ratios between 40:1 and 4:1. In contrast, for cocultures with higher

proportion of EC, endothelial clustering followed by apoptosis was detected. Moreover, in both 40:1 and 20:1 cocultures, the fibroblast-to-HUVEC ratio declined over time, stabilizing by day 15 in the range of 10 to 1. These pioneering findings, led Kunz-Schughart *et al.*[101] to suggest that vascular patterning in networks strongly depends on an optimal cell ratio. In other words, an optimal balance of heterotypic interactions is necessary, in which low percentages of EC seems to favor heterotypic communication towards the formation of primitive vascular networks[101]. These results were later confirmed by Rouwkema *et al.*[95], who reported that by seeding 2% or fewer HUVEC, the formation of a 3D prevascular network was promoted within 10 days in MSC-HUVEC coculture spheroids.

Apart from that, other physical and biochemical factors have been related to vascular patterning in coculture spheroids. For example, Saleh *et al.*[102] suggested that the spheroid size might have an effect on vascular patterning, due to the mechanical gradient prevailing in larger spheroids. In that study, Saleh *et al.*[102] reported the formation of OB-HUVEC spheroids, where EC were located in the innermost areas while OB were predominantly at the periphery. Contrary to these results, Stahl *et al.*[96] reported the opposite patterning for the same type of spheroids, but with 60 times less cells. As so, this difference might have arisen as mechanical forces induced cell patterning in different ways depending on the spheroid sizes.

Taking into account the several physical and biochemical factors described above, it is clear that vascular patterning within coculture spheroids is a complex and dynamic process, which is far from being totally understood. Considering that different types of vascular microstructures within spheroids may exhibit distinct angiogenic potentials when implanted *in vivo*, more efforts should be employed in understanding vascular patterning in coculture spheroids.

Chapter II

Materials and Methods

II.1. Primary human cell sources

Human bone marrow MSC (PT-2501, Lonza) were cultured using T175 cm^2 flasks in Dulbecco's Modified Eagle Medium (DMEM, Gibco) containing 10% v/v fetal bovine serum (FBS) (Hyclone, GE Healthcare) and 1% v/v penicillin/streptomycin (P/S) (Gibco). Culture medium was changed every 3 to 4 days. OEC were isolated from human umbilical cord blood of healthy donors, as described elsewhere[103], and were a kind gift from Eduardo Silva Lab (UC Davis UCB collection program). OEC were routinely cultured using T75 cm^2 flasks in Microvascular Endothelial Cell Growth Medium (EGM-2MV) (Lonza) and 1% v/v P/S) (Gibco). Culture medium was changed every 2 to 3 days. Both cell types were grown at 37°C under a 5% v/v CO_2 humidified atmosphere.

II.2. Generation of monoculture and coculture spheroids

II.2.1. Preparation of agarose microwell arrays

Spheroids were obtained by using commercially available micromolds (MicroTissues, Inc) for casting agarose microwell arrays (3D Petri Dishes) (**Fig.5**). The microwell arrays were prepared according to manufacture specifications. Briefly, agarose (SeaKem® LE Agarose, Lonza) was sterilized (autoclave, 30 min at 140°C) and dissolved in 0.9% w/v NaCl at a final concentration of 2% w/v under microwave heating. The molten agarose was filtered (0.2 μm, filtropur S0.2, Sarstedt) and 500 μL of agarose solution were poured into each micromold. After gelling, the casted microwell arrays were carefully transferred to a 12-well plate (353043, Falcon®) and equilibrated with EGM-2MV medium overnight (ON).
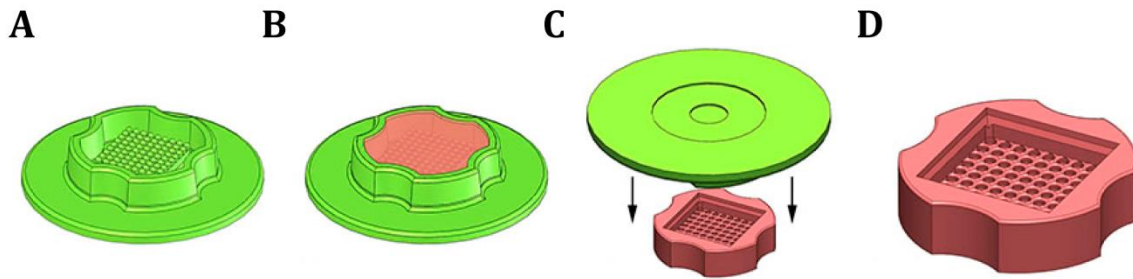
Figure 5 - Fabrication of microtissue spheroids. (A) Commercially available precision mold; (B) Mold filled with molten agarose; (C) Release of the microwell array; (D) Final microwell array of gelled agarose (800 μm diameter microwells, 9x9 arrays). Original flow chart retrieved from Microtissues, Inc. website.

II.2.2. Cell seeding into microwell arrays

The agarose multiwell arrays were used to generate spheroids as previously described[30,31]. Here, MSC, OEC and OEC-MSC (1:1 cell ratio) spheroids were prepared. After expansion, cells between passage 6 and 8 were tripsinized when reaching 70 to 80% confluence, counted using a Neubauer chamber, centrifuged (1200 rpm, 5 min) and resuspended at the desired concentration. Culture medium was removed from the agarose microwell arrays and loaded with 190 μL of cell suspension at a final concentration of 3.24×10^5 cells per array, yielding ca. 4000 cells per spheroid. Cells were allowed to settle down for 10 or 30min at room temperature (RT). After that, 1.5 mL of EGM-2MV were added to the outside of the microwell arrays and incubated at 37°C. Medium was changed every 2 to 3 days and spheroids were collected for analysis at day 1, 4, 7 and 14.

II.3. Analysis of monoculture and coculture spheroids

II.3.1. Cell viability and metabolic activity assays

To detect viable cells and their spatial localization within the spheroids, spheroids were stained using a standard live/dead assay. Briefly, cell culture medium was replaced by 4 μM Calcein AM (C-1430, Invitrogen) solution diluted in prewarmed PBS. Spheroids were incubated at 37°C for 30min, washed twice with PBS and incubated with 6 μM Propidium Iodide (PI, P4170, SIGMA) at 37°C for 10 min and washed again twice with prewarmed PBS. Spheroids were resuspended in DMEM without phenol red (Gibco), placed into a glass bottom 35 mm Petri dish (MatTek Corporation, USA) and immediately imaged by using Leica TCS SP5

inverted confocal microscope. Calcein AM stains live cells with esterase activity in green, while PI stains cells with compromised membranes (unviable) in red.

Resazurin assay was used to analyze spheroids metabolic activity. This assay is based on the ability of metabolically active cells to reduce resazurin (dark blue with little fluorescence) into resorufin (pink and highly fluorescence) generating a fluorescent signal. At pre-defined time points, samples from 3 microwell arrays (8-15 spheroids each) were collected and transferred to a 96-well plate. Resazurin (R7017, SIGMA) was diluted in fresh EGM-2MV medium to a work dilution of 20 µg/mL, added to the spheroids and incubated for 2h at 37°C. Supernatant was transferred to a 96-well black plate and fluorescence was measured in a microplate reader (Synergy Mx, BioTek) at 530nm/590nm (EX/EM) wavelengths. Replicates were normalized to the number of spheroids.

II.3.2. Histology and Immunohistochemistry

For histological and immunohistochemical analysis, spheroids were fixed directly inside the agarose arrays using 4% w/v paraformaldehyde (PFA) (15713, EMS) in PBS for 30min at RT and washed 3X with PBS. Thereafter, 200 µL of molten HistoGel™ (HG-4000-012, ThermoFisher) were added to the array chamber to prevent loss of spheroids during further processing. After gelling, arrays were placed inside histological cassettes, immersed in PBS and processed using an automatic rotational tissue processor (STP-120-1, MICROTOM). Tissue processing was set to graded series of 1h each, starting by sequential immersion in ethanol (EtOH) solutions of increasing concentrations (70%, 90%, 98% and 3X in 100%), followed by 3X immersion in ClearRite 3 and finally 2x immersion in preheated paraffin. Arrays were then paraffin-embedded in an EC-350 embedding centre. Paraffin blocks were cut in a Leica RM2255 microtome into 3 µm and 6 µm sections for histological and immunohistochemical analysis, respectively. Paraffin-embedded sections were mounted on (3-aminopropyl)triethoxysilane (APES) (440140, SIGMA)-coated glass slides, dried ON at 37ºC and then kept at RT until use.

Hematoxylin/Eosin (H&E) staining was used for spheroid morphological analysis. Paraffin sections were deparaffinized in xylene 3X for 5min each, rehydrated in 100%, 96%, 70% and 50% EtOH dilutions series for 10 min each and finally washed in distilled water. Sections were then immersed in Gill's Hematoxylin solution (GHS232, SIGMA) for 2.5 min followed by rising in running tap water for 3min. Sections were dehydrated using a series of EtOH solutions (50%, 70%, 96% and 100%, for 10 min each), followed by staining in alcoholic eosin (Y 515,

Leica) solution for 2-4 min. Sections were then washed 3X in EtOH 100% solution followed by 3X immersion in a xylene bath, and finally mounted with Entellan® mounting medium (107961, Merck). Images at single focal plane were taken using a Zeiss Axioskop 2 microscope.

For immunohistochemistry, paraffin-embedded sections were incubated at 50ºC for 30min and then deparaffinized and rehydrated as performed for the H&E staining. Slides were then immersed in 1X PBS for 30min. For antigen retrieval, spheroid sections were incubated in water bath at 96ºC for 30 min in freshly prepared 10 mM sodium citrate buffer, pH=6 or 10 mM Tris-1 mM EDTA (TE) buffer, pH=9. Sections were then kept in the antigen retrieval solutions for 20 min at RT and washed 3X in PBS for 5 min each. Samples were permeabilized in PBS 0.25% v/v Triton™ X-100 (X100, SIGMA) for 10 min under agitation followed by blocking in PBS supplemented with 5% v/v FBS for 1h at RT. Primary antibody incubations (**Table 1**) were prepared in PBS supplemented with 2.5% v/v FBS O.N at 4ºC. Sections were then washed 3X in PBS for 5 min each, secondary antibodies were prepared as for the primary antibodies and incubated for 1h at RT, including 3X washes in PBS for 5 min each at the end. Depending the assay, the following fluorochrome-conjugated secondary antibodies were used: Alexa Fluor® 488 goat anti-rabbit (A11008, ThermoFisher), Alexa Fluor® 594 goat anti-mouse (A11020, ThermoFisher) (1:1000); Alexa Fluor® 647 goat anti-rabbit (A11072, ThermoFisher) (1:500). Nuclei were stained with 4',6-diamidino-2-phenylindole (DAPI) diluted in PBS 0.05% v/v Tween 20 for 10 min. Slides were then mounted using VectaShield (H-1000, Vector) antifade mounting medium. Z-series optical sections were collected using a Zeiss AxioImager Z1 (Carl Zeiss, Germany) equipped with an AxioCam MR ver.3.0.

Table 1 – Primary antibodies used for immunohistochemical analysis. atypical protein kinase C (aPKC); Tight junction protein 1 (ZO-1).

Targeted antigen	Species source	Reference	Manufacturer	Antibody dilution	Antigen retrieval buffer	
					Citrate	TE
Fibronectin	Rabbit	F3648	SIGMA	1:200	Yes	No
Laminin	Rabbit	L9393	SIGMA	1:100	No	No
Collagen IV	Mouse	CIV22	Dako	1:100	No	Yes
CD31	Mouse	M0823	Dako	1:150	Yes	Yes
CD144	Mouse	sc-9989	Santa Cruz	1:100	No	Yes
vWF	Rabbit	A0082	Dako	1:300	Yes	Yes
CD105	Mouse	555690	BD	1:100	No	No
CD90	Sheep	AF2067	R&D	1:50	No	No
aPKC	Rabbit	Ab32376	Abcam	1:200	No	No
ZO-1	Rabbit	61-7300	Thermofisher	1:200	No	No
Ki67	Rabbit	Ab15580	Abcam	1:800	Yes	No

II.3.3. Immunofluorescence analysis of whole mount processed spheroids

To analyze spatial cell distribution and ECM deposition in 3D, spheroids were retrieved from agarose molds and analyzed as whole-mount samples. Spheroids were washed 3X with PBS, fixed in 4% v/v PFA in PBS or 30min at RT and washed in 1X PBS for 10min. Spheroids permeabilization was performed in PBS with 0.25% v/v Triton™ X-100 for 30 min followed by blocking in PBS supplemented with 1% w/v bovine serum albumin (BSA) for 1h at RT. Primary antibody incubation with anti-human CD31 (1:50) and anti-human fibronectin (1:100) was performed ON at RT, under constant agitation. After washing 3X with PBS, for 15 min each, spheroids were incubated with the respective secondary antibodies, Alexa Fluor® 594 goat anti-mouse (1:500) and Alexa Fluor® 647 goat anti-rabbit (1:500). For f-actin staining, samples were incubated with Alexa Fluor 488 Phalloidin (Life Technologies) (1:50) for 4h at RT. Immunostained spheroids were then washed 3X with PBS, for 15 min each, and finally mounted with Vectashield mounting medium with DAPI (Vector Laboratories, Inc Burlingame, CA 94010). Images were acquired using a Leica TCS SP5 AOBS spectral confocal microscope (Leica Microsystems,Germany).

II.3.4. Flow cytometry analysis

For flow cytometry analysis of OEC to MSC ratios over time, coculture spheroids collected at different time points were mechanically and enzymatically dissociated. A defined number of spheroids (180-240 for each timepoint) were transferred to 1.5 mL eppendorfs, washed with pre-warmed PBS and incubated for 15 min in pre-warmed TrypLE Express (12605028, Gibco) solution containing 1.5 U/mL of Dispase® II (10374300, Roche) in a thermomixer rotating, at 37°C and 1050 rpm. The enzymatic solution was then replaced by TrypLE Express containing 200 μg/mL of crude collagenase (C0130, SIGMA) and samples were further incubated for 15 min. After spheroids disaggregation, cells were washed with prewarmed PBS, centrifuged and resuspended at appropriate concentration in FC buffer (0.01% w/v sodium azide, in PBS with 0.5% w/v BSA). Cell suspensions ($1x10^5$ cells in 50 μL) were stained for 1h at 4ºC in the dark with FITC-labeled anti-human CD31 (555445, BD) (1:25) and APC-conjugated anti-human CD90 (eBio5E10, eBiosciences) (1:20). Stained cells were resuspended in cold PBS and analysed under FACS Calibur machine. PI (1 μg/mL) was added 1-2 minutes before the analysis to exclude non-viable cells. Data was analysed using the software FlowJo v10. A minimum of 10,000 events were analysed for each dot plot. Firstly, cells were separated from debris using the scatter plot and then PI^{+} cells were excluded. Single APC and FITC samples were used to define the gates.

II.3.5. Statistical analysis

Statistical analyses were performed using GraphPad Prism 5 software version 5.03. The unpaired student's *t*-test was used to compare two groups of data that followed a parametric distribution, whereas the Mann-Whitney test was performed for non-parametric data. A value of $p < 0.05$ was considered statistically significant.

Chapter III

Results

III.1. Scalable spheroid generation and analysis

In the present study, MSC and OEC were cultured in nonadhesive microwell arrays cast from autoclavable precision molds (Microtissues, Inc). The use of this platform allowed the scale up of essentially monodispersed spheroids at 81 units per mold (**Fig.6A**). Herein, spheroids were directly embedded in paraffin without being removed from the microwells. This approach enabled the presence of several spheroids per section in an orderly distributed manner (**Fig.6B, C**). However, it should be noted that only a fraction of spheroids were still present in paraffin-embedded sections (**Fig.6B, C**). Nevertheless, this approach enabled a HT histological and immunohistochemistry analysis.
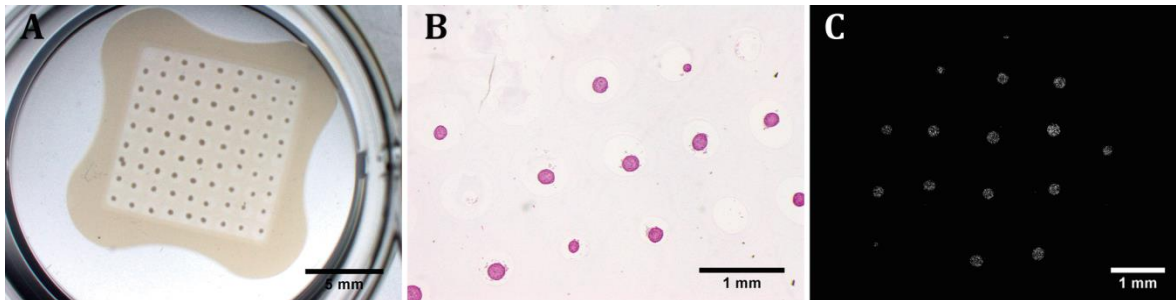
Figure 6 - HT formation of spheroids using the precision molds (Microtissues, Inc). (A) Brightfield image of a microwell array loaded with 81 spheroids and placed inside a standard 12-well plate; (B, C) H&E and DAPI in 3μm paraffin-embedded sections, respectively. Brightfield and fluorescence images acquired using a 5x magnification.

III.2. Morphology of assembled spheroids

To study the spatial organization of EC and potential to assemble prevascularized spheroids, MSC and OEC were combined at a 1:1 cell ratio and cultured in microwell arrays for up to 14 or 21 days. Additionally, MSC and OEC were individually cultured under the same conditions in order to obtain the respective monoculture spheroids, which were used as controls. Within

24h, cells on both mono- and cocultures were able to spontaneously aggregate into spheroids that remained intact along the culture period (**Fig.7A, B**). Cell compaction took place during the first hours of culture, after which spheroid size was maintained between approximately 230 μm and 260 μm in diameter, with no significant differences between mono- and cocultures (**Fig.7B**). Since, in the first two experiments it was observed that a substantial amount of cells still remained in suspension after an incubation period time of 10 min, a 30 min period time was used in the following experiments, which resulted in an improved cell suspension deposition. Nevertheless, both time points led to the assembly of spheroids with similar size (**Fig.7B**). An incubation time of 30 min was adopted thereafter for both mono- and coculture spheroids.

As highlighted in **Fig.7C**, MSC and MSC-OEC cocultures were able to assemble into compact spheroids, whereas OEC monoculture formed irregular and loose spheroids that easily dissociated when subjected to cell culture manipulation, making further analysis nearly impossible. Also, by day 4, in opposition to monocultures, MSC-OEC spheroids were found to develop an external layer of cells surrounding the spheroid compact mass, suggesting that some cells detached over time. This was further confirmed by immunohistochemical analysis, showing also that most cells in this cell corona were OEC, as they stained positive for the specific endothelial surface marker CD31 in paraffin-embedded sections.
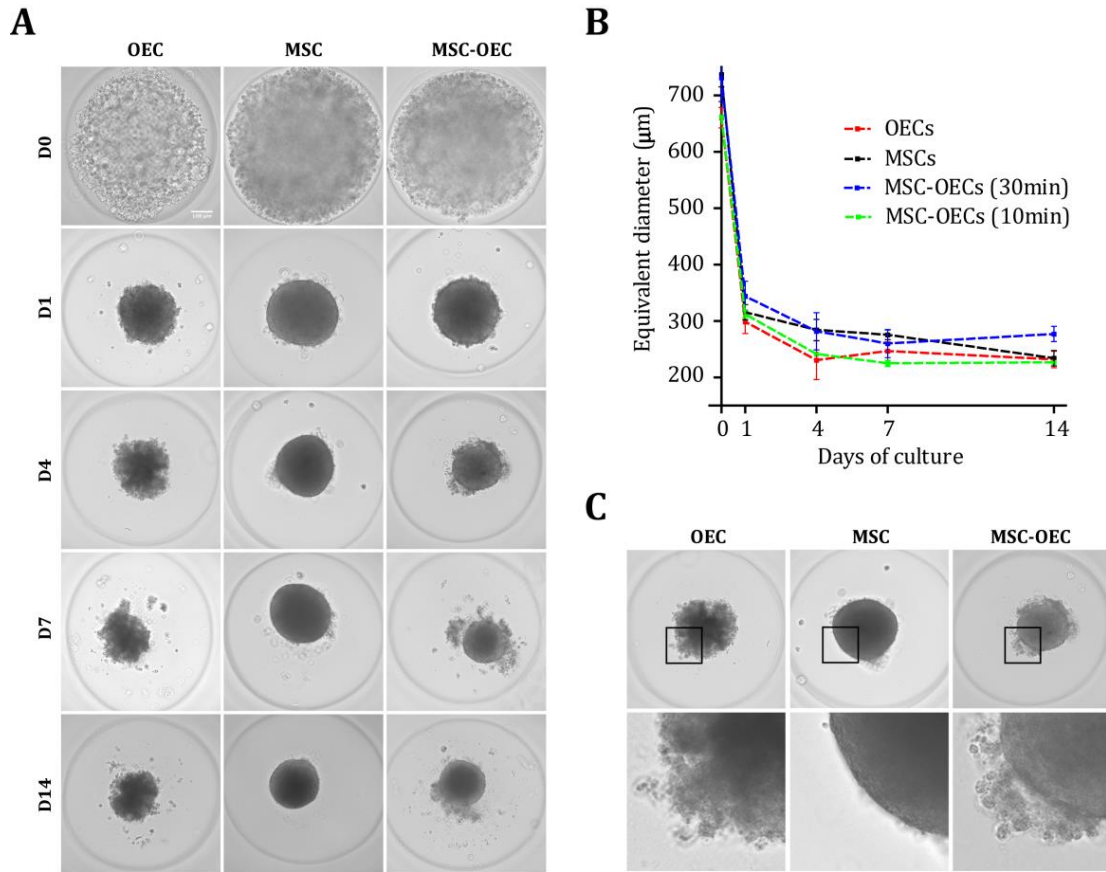
Figure 7 – Assembly of OEC and MSC into mono- and coculture spheroids. (A) Brightfield images of OEC, MSC and MSC-OEC spheroids at different time points (0, 1, 4, 7, 14 days). Images in day 0 were acquired 30 min after seeding. (B) Spheroid diameter was determined by outlining spheroid area in brightfield images using ImageJ software; (C) OEC, MSC and MSC-OEC spheroids at day 4. Spheroid corona is highlighted for each spheroid cell type. Brightfield images acquired using a 40x magnification. Insets, 3x. Scale bar 100 μm.

H&E staining was performed to further assess the morphology and structure of spheroids at the established time points. At day 1, MSC and MSC-OEC spheroids showed a well-defined circular structure, while OEC spheroids were found to adopt an irregular shape (**Fig.8**). By day 4, OEC spheroids were not able to withstand paraffin processing and eventually dissociated. Therefore, no further data was possible to acquire for OEC spheroids.

At day 1, in MSC and MSC-OEC spheroids, cells were randomly dispersed throughout the spheroid (**Fig.8A, B**). Yet, after 4 days of culture, two morphologically different areas could be identified within spheroids, namely an outer layer composed of elongated cells and a central region predominately composed of randomly distributed round-shaped cells (**Fig.8C, D**). At the end of day 7, MSC spheroids showed a higher nuclei/ECM ratio than coculture spheroids

(**Fig.8E, F**). Since, both spheroid types have similar sizes; this suggests that there was a loss of cells in coculture spheroids throughout culture.
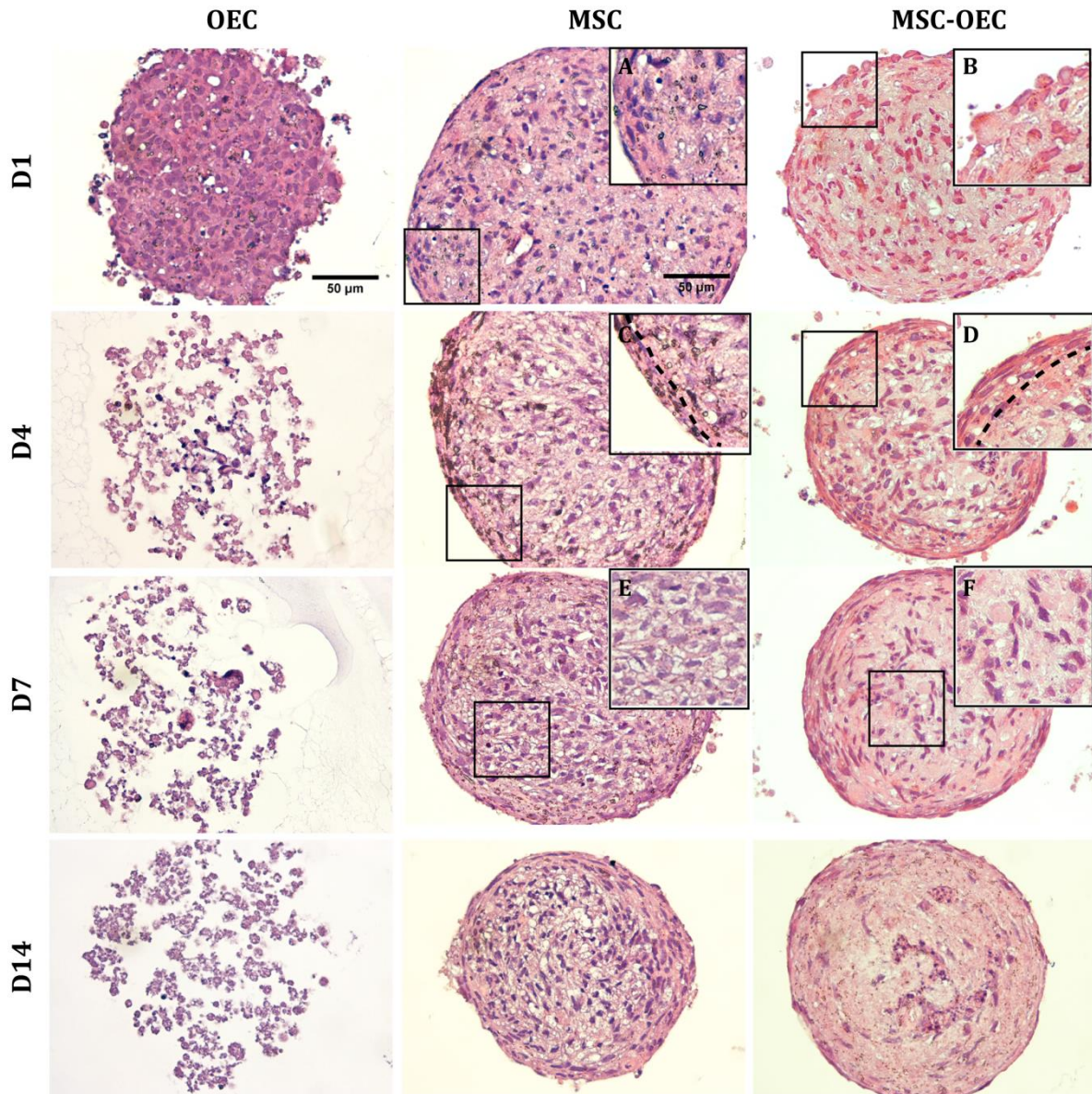

Figure 8 – Spheroids tissue morphology. H&E staining in 3 μm paraffin-embedded sections of OEC, MSC and MSC-OEC spheroids. (A-F) – Amplification of different external and inner regions of spheroids are depicted in insets. Optical images were acquired using a 40x magnification. Insets, 2x. Scale bar 50 μm.

III.3. Cell viability, metabolic activity and proliferation

Taking into consideration that a dense 3D microenvironment may interfere with cellular activity, namely by reducing the access to nutrients and oxygen in the innermost parts[32,104], cell viability, metabolic activity and proliferation were assessed at the different time points.

Viable and nonviable cells were detected in live spheroids stained, respectively, with Calcein AM and PI under a confocal microscope. No fluorescence signal was possible to acquire in the innermost areas of the spheroid (**Fig.9A**). This technical problem was observed for all time points and, therefore, no valid conclusions could be taken regarding cell viability in live spheroids.

The metabolic activity was determined for MSC and MSC-OEC spheroids using the resazurin assay. Between days 1 and 4 the metabolic activity decreased significantly for both MSC and MSC-OEC spheroids (**Fig.9B**), while from day 4 forward it remained almost constant (**Fig.9B**). Since, for MSC spheroids, only one single experiment was performed, no statistical analysis could be carried out. However, for the coculture spheroids, the initial decrease observed in the metabolic activity was statistically significant ($p < 0.001$).

The percentage of proliferative cells was quantified for coculture spheroids in paraffin-embedded sections as the number of Ki67+ nuclei in relation to total nuclei. Similar to what was observed for metabolic activity, a 3-fold decrease of the number of proliferative cells was determined during the first 4 days, with 13% of the total cells expressing Ki67 by day 1, and only 2% Ki67+ cells being detected at day 4 (**Fig.9C**). While, a slight increase was observed at day 7, only 1% Ki67+ cells were detected at day 14. In terms of spatial distribution, proliferating cells were found to be randomly distributed throughout the spheroid at day 1 (**Fig.9D**), but after 4 days these were predominately located at the most peripheral layers.
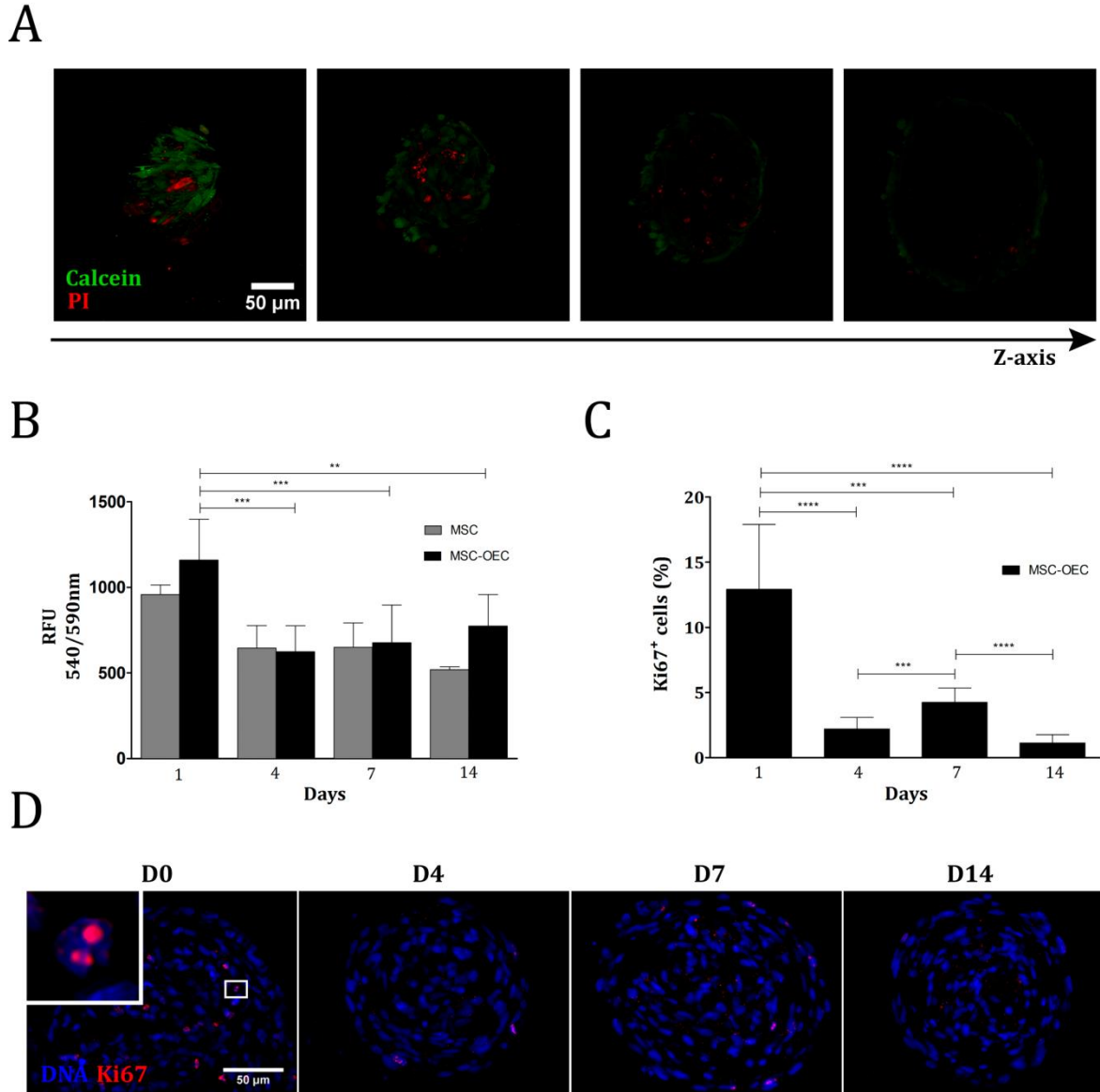
Figure 9 – Spheroids cell activity. (A) Calcein /PI Live dead assay. Images represent sequential 2 μm Z planes of a 24h whole coculture spheroid incubated with calcein (live cells) followed by PI (dead cells). Dead cells are shown in red and live cells in green (B) Cell metabolic activity for MSC (n=3, from 1 independent experiment) and MSC-OEC spheroids (n=12, from 3 independent experiments). RFU stands for relative fluorescence units; (C) Cell proliferation ratio for MSC-OEC spheroids. Quantitative results are presented as mean ± standard deviation (SD). The Man-Whitney test was used to compare two groups, ** $p < 0.01$, *** $p < 0.001$, **** $p < 0.0001$. (D). Immunocytochemistry for Ki67+ cells within spheroids. Cells were immunostained with Ki67 to depict proliferative cells (red) and incubated with DAPI to stain DNA (blue). Images were taken using a 40x magnification objective. Inset, 8x. Scale bar 50 μm.

III.4. ECM deposition

The ECM is well known to be a critical factor for cell survival and maintenance after implantation[3,105]. However, its structure and function in prevascularized spheroids remains largely uncharacterized. Herein, the expression of two ECM proteins, collagen type IV and FN was assessed.

Collagen type IV and FN expression was barely detectable within OEC spheroids at day 1 (**Fig.10B, C**). Both MSC and MSC-OEC spheroids were found to express collagen type IV, which formed an extensive meshwork throughout the microtissue (**Fig.11**). However, for coculture spheroids, type IV collagen fibers were present from day 1, where for MSC spheroids, it was only detected after 4 days of culture (**Fig.11**). Moreover, type IV collagen fibers assembled over time into an outer layer of aligned fibers surrounding a more disorganized core. Such assembly was found to be more pronounced in MSC-OEC spheroids than in MSC monocultures (**Fig.11**). FN deposition was also detected in MSC and MSC-OEC spheroids (**Fig.12**). For MSC spheroids, FN remained mainly non-polymerized throughout culture, although some fibers inside the spheroid tissue were observed by day 7 and 14 (**Fig12**). Contrarily, in MSC-OEC spheroids, a FN meshwork of elongated fibers was assembled at the periphery. FN expression was barely detectable in the inner regions of the spheroid (**Fig12**).
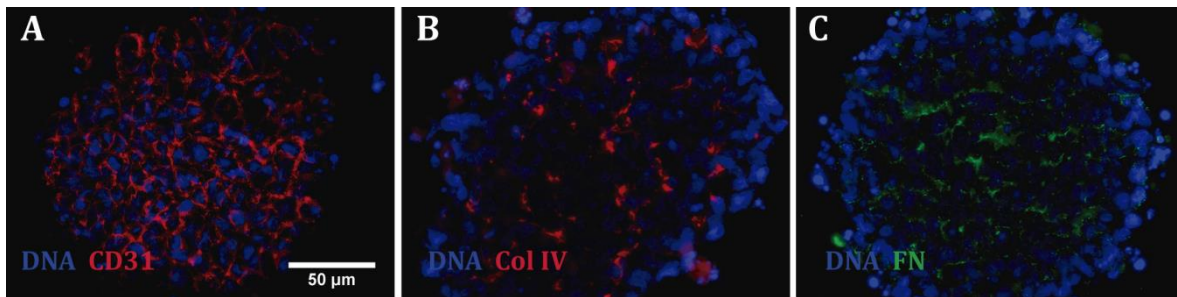
Figure 10 – Collagen type IV and FN expression within OEC spheroids. (A) Organization of OEC stained against the expression of CD31; (B, C) Immunostaining of collagen type IV (red) and FN (green) counterstained with DAPI (blue). Images were taken with a 40X objective. Scale bar 50 µm.
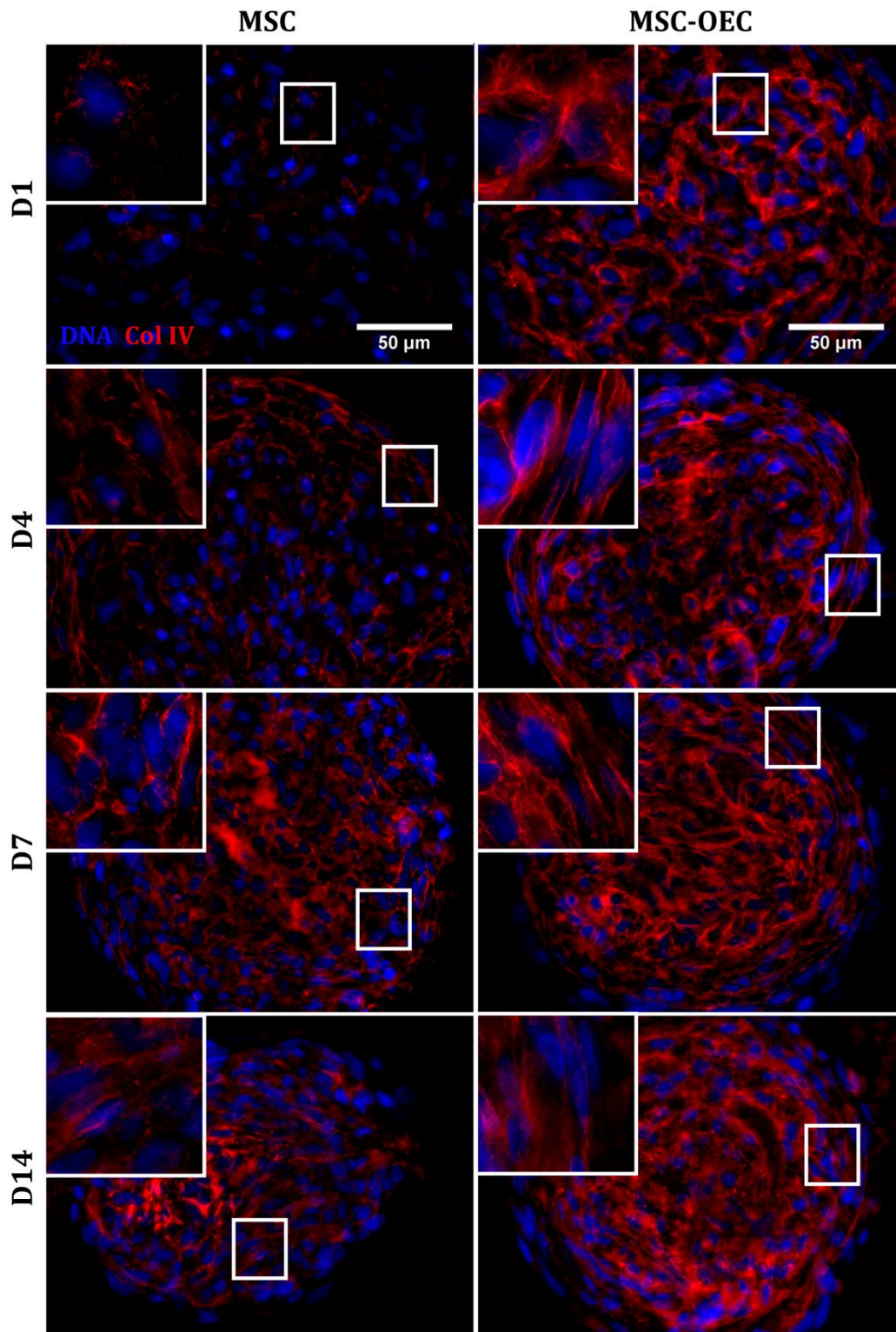
Figure 11 – Spatial localization of type IV collagen in spheroids. Immunostaining of collagen type IV (red) and counterstained with DAPI (blue) in 6 μm paraffin-embedded sections of MSC and MSC-OEC spheroids. Images were taken with a 40X objective. Insets 3x. Scale bar 50 μm.

Figure 12 – FN deposition and distribution in spheroids. Immunostaining of FN (green) and counterstained with DAPI (blue) in 6 μm paraffin-embedded sections of MSC and MSC-OEC spheroids. Images were taken with a 40X objective. Insets 3x. Scale bar 50 μm.

III.5. Endothelial organization in coculture spheroids

III.5.1. OEC patterning and OEC-to-MSC ratio

One of the main goals of the present study was to characterize the 3D spatial organization of OEC in coculture spheroids. The first approach was to stai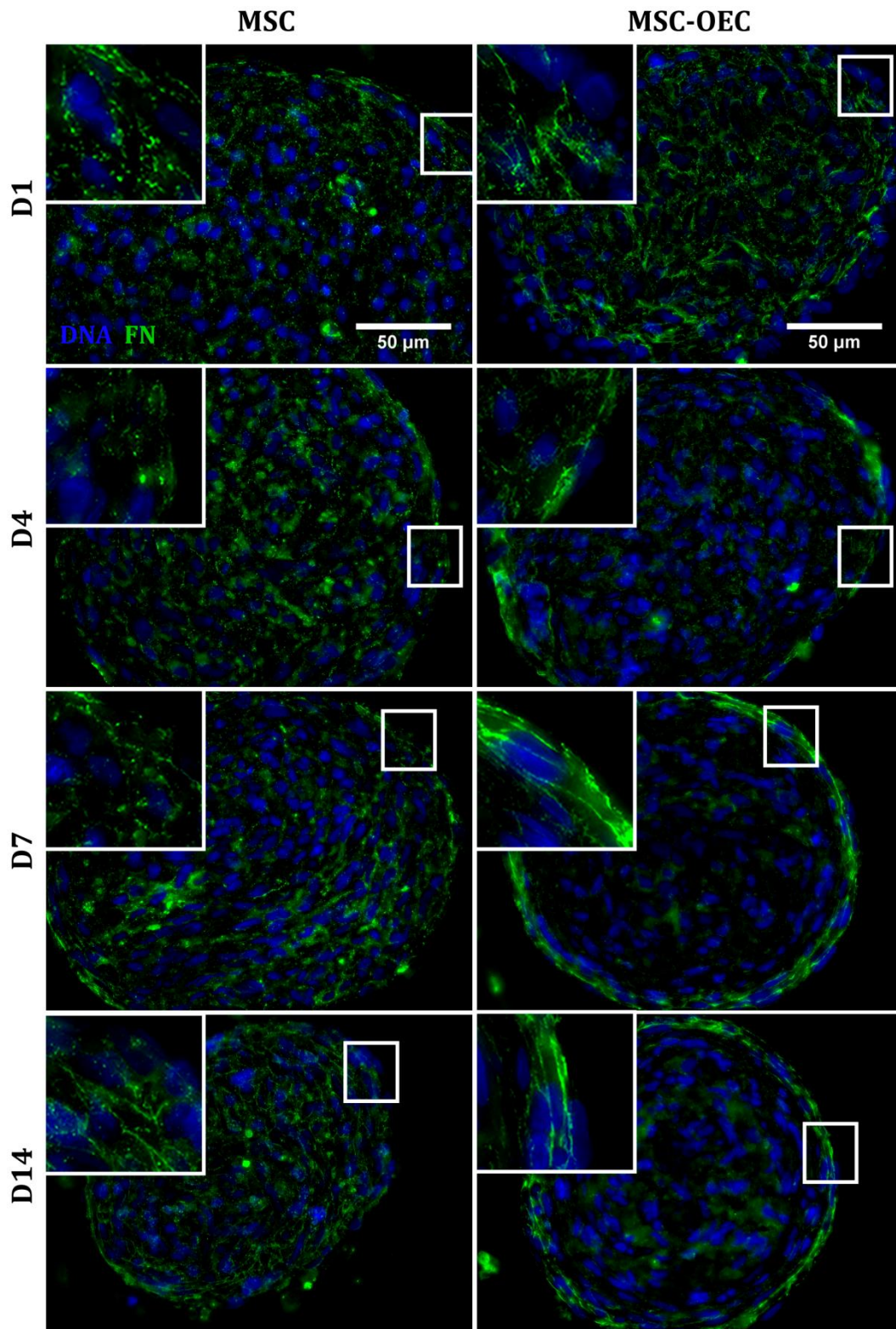n the whole MSC-OEC spheroid for the expression of EC-marker CD31 and imaged it through confocal microscopy. Similarly to what occurred in the live/dead assay, CD31 signal for the innermost areas of the spheroid was not possible to acquire (**Fig.13A**). In order to enhance tissue transparency, spheroids were cleared before visualization using a detergent- and solvent-free clearing method (Clear[T2]). This optical clearing protocol was previously reported to improve fluorescence signal collection in whole spheroids[76,106]. However, in the present study, Clear[T2] protocol did not significantly increase CD31 signal acquisition (data not shown).

In alternative, OEC spatial distribution was assessed by staining spheroids for the expression of CD31 in paraffin-embedded sections. As a control, expression of CD31 was also analyzed in MSC spheroids but it was barely undetectable. For cocultures, spheroids spontaneously organized into a continuous surface monolayer of OEC surrounding an MSC-enriched core with some OEC entrapped inside (**Fig.13B**). While this surface monolayer remained intact throughout culture, after 4 days, the amount of OEC inside the spheroid apparently decreased **(Fig13B)**.

A

Whole spheroids

DNA CD31

50 μm

Z-axis

B

Paraffin-embedded sections

D1 D4 D7 D14

MSC

DNA CD31 50 μm

MSC-OEC

50 μm
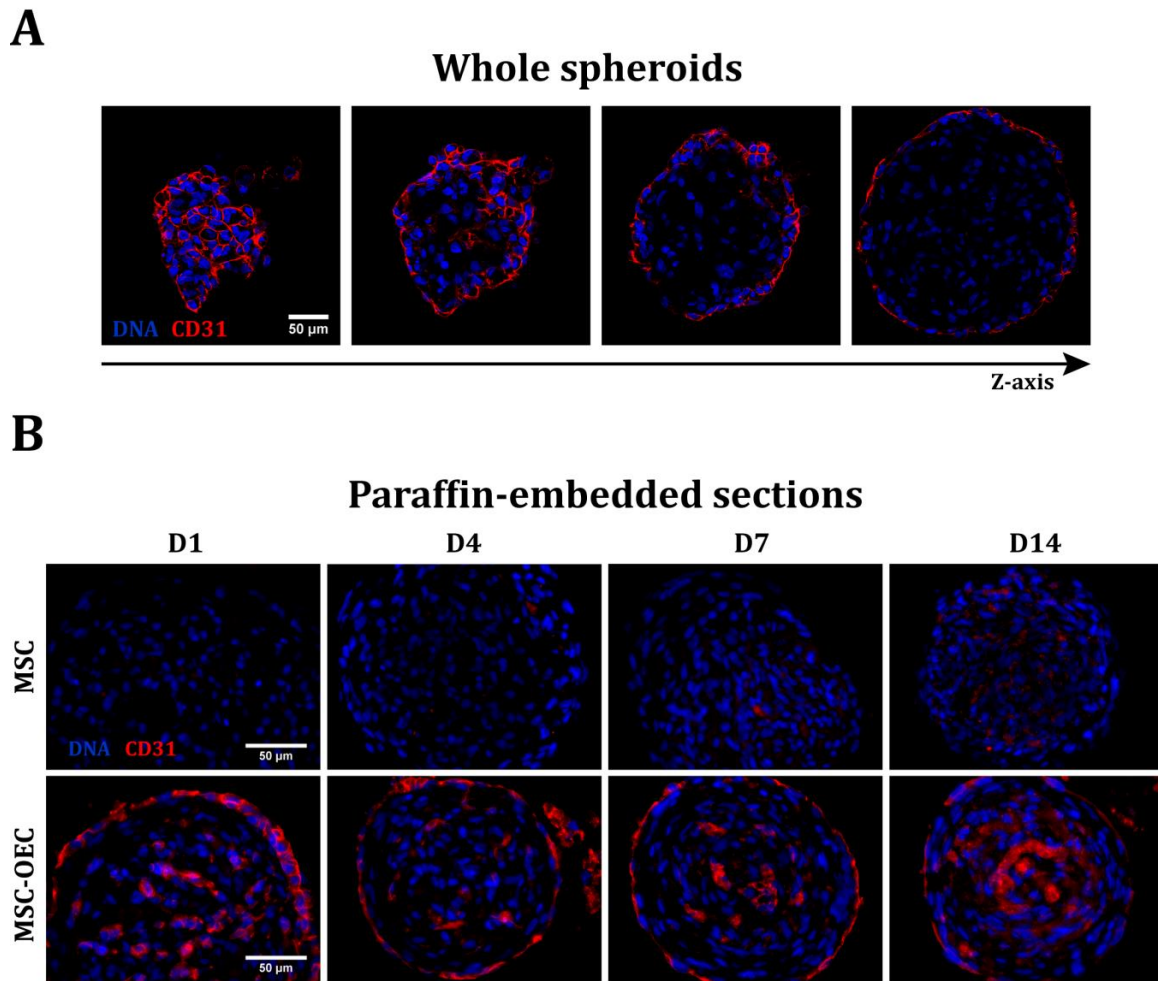
Figure 13 – CD31 expression and organization in coculture spheroids. (A) Immunostaining of CD31 (red) in whole spheroid counterstained with DAPI (blue). Z axis direction from the periphery to core of the spheroid. (B) CD31 staining was used to assess endothelial organization in 6 um paraffin embedded sections. Images were acquired using a 40x objective. Scale bar 50 μm.

Sections stained against the expression of CD31 showed that OEC remaining inside spheroids did not organize into primitive vascular networks. Rather, OEC formed small cellular clusters at the core that become more evident over time, both in number and in size (**Table 2**).

Table 2 – OEC clustering in MSC-OEC spheroids. Cellular clusters were divided into three different classes according to their size. The number of sprouts was also quantified. Cumulative numbers from n=15 of one biological experiment.

Day	Cluster size			Number of sprouts
	<100μm^2	100μm^2-300μm^2	> 300μm^2	
1	0	0	0	-
4	14	0	0	3
7	35	12	1	9
14	15	19	1	19

In order to confirm the loss of OEC, the relative amount of the two cell types was quantified by staining for the expression of CD31 in paraffin-embedded sections and by flow cytometry. Quantification of OEC in sections revealed a MSC to OEC ratio of ca. 1:1 ± 0.21:1 at day 1, while for the following days it significantly (P<0.0001) increased to 4:1 ± 0.65:1, 8:1 ± 0.89:1 and 20:1 ± 1.06:1 at days 4, 7 and 14, respectively (**Fig.14A**). Indeed, ~72-82% of the seeded OEC were lost during the first 4 days of culture, whereas ca. 95% ± 1% of OEC disappeared since the starting until the end of the experiment. Additionally, spheroids were collected, dissociated and analyzed using flow cytometry. By using FITC-conjugated CD31 antibody and APC-conjugated CD90, OEC and MSC populations were possible to be distinguished in the FL1 vs FL2 dot plot (**Fig.14B)**. Membrane-damaged cells were excluded from the results by PI staining. Similar MSC to OEC ratios were obtained at day 1 (1,8:1) and day 4 (4:1). Yet, unexpectedly, a recovery in the relative amount of OEC was detected by day 7, which has not been observed by image quantification.
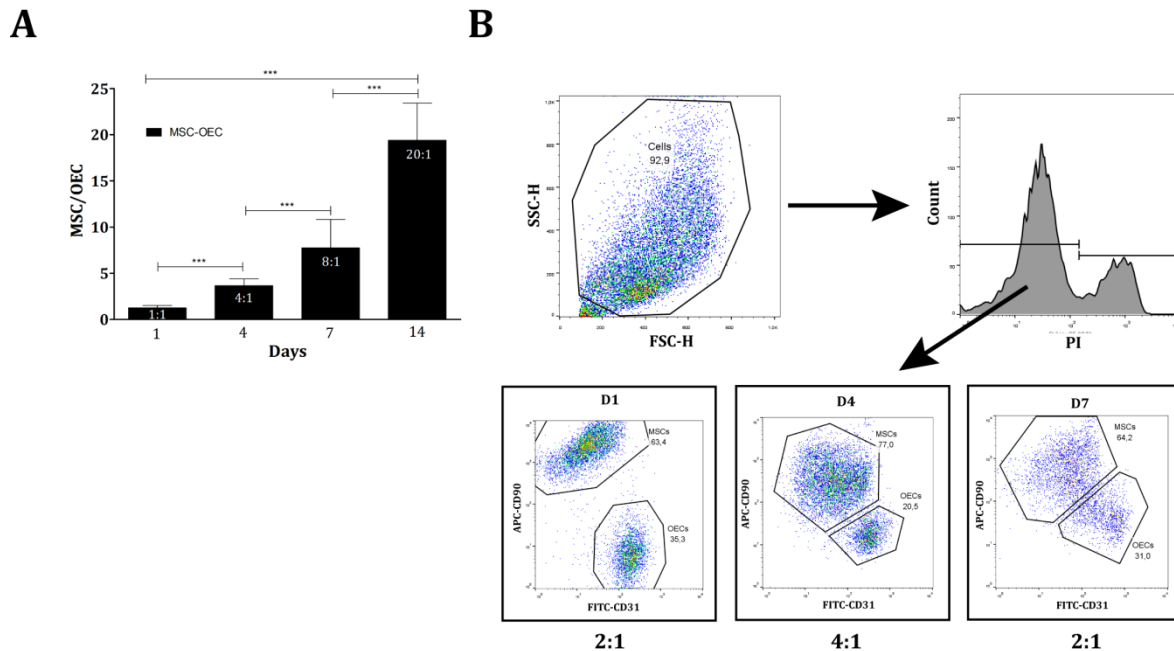
Figure 14 – Quantification of MSC:OEC ratio in spheroids throughout time. (A) Quantification of CD31 positive cells in paraffin-embedded sections. Results are presented as mean ± SD (n=10, from one independent experiment). *** p<0.0001 as determined by the student t-test. (B) Quantification of cell ratios for day 1, 4 and 7 by flow cytometry. MSC-OEC ratios are display below the plots.

III.5.2. Endothelial surface monolayer

In order to further study the organization and phenotype of OEC in the surface monolayer, whole spheroids were stained for the expression of CD31 and then visualized under confocal microscopy. Z-stack projections of the spheroid surface revealed that, after 24h, OEC assembled into a tightly packed capsule with well-defined cell-cell contacts observed through CD31 expression. (**Fig.15**). Over time, OEC elongation was observed, resulting in an aligned monolayer entrapping an enriched MSC core. This was further confirmed in paraffin-embedded sections. While, OEC at the periphery initially adopted a cuboidal shape, a flattened morphology was more evident over time (**Fig.16A**). The thickness of the endothelial surface monolayer significantly decreased (P<0.001) throughout time, from 26 µm ± 0.72 µm at day 1 to 9 µm ± 0.51 µm at the end of the experiment (**Fig.16B**). Moreover, this morphological change was accompanied by a significantly decrease (P<0.001) in the amount of OEC at the periphery (**Fig.16C**).

34
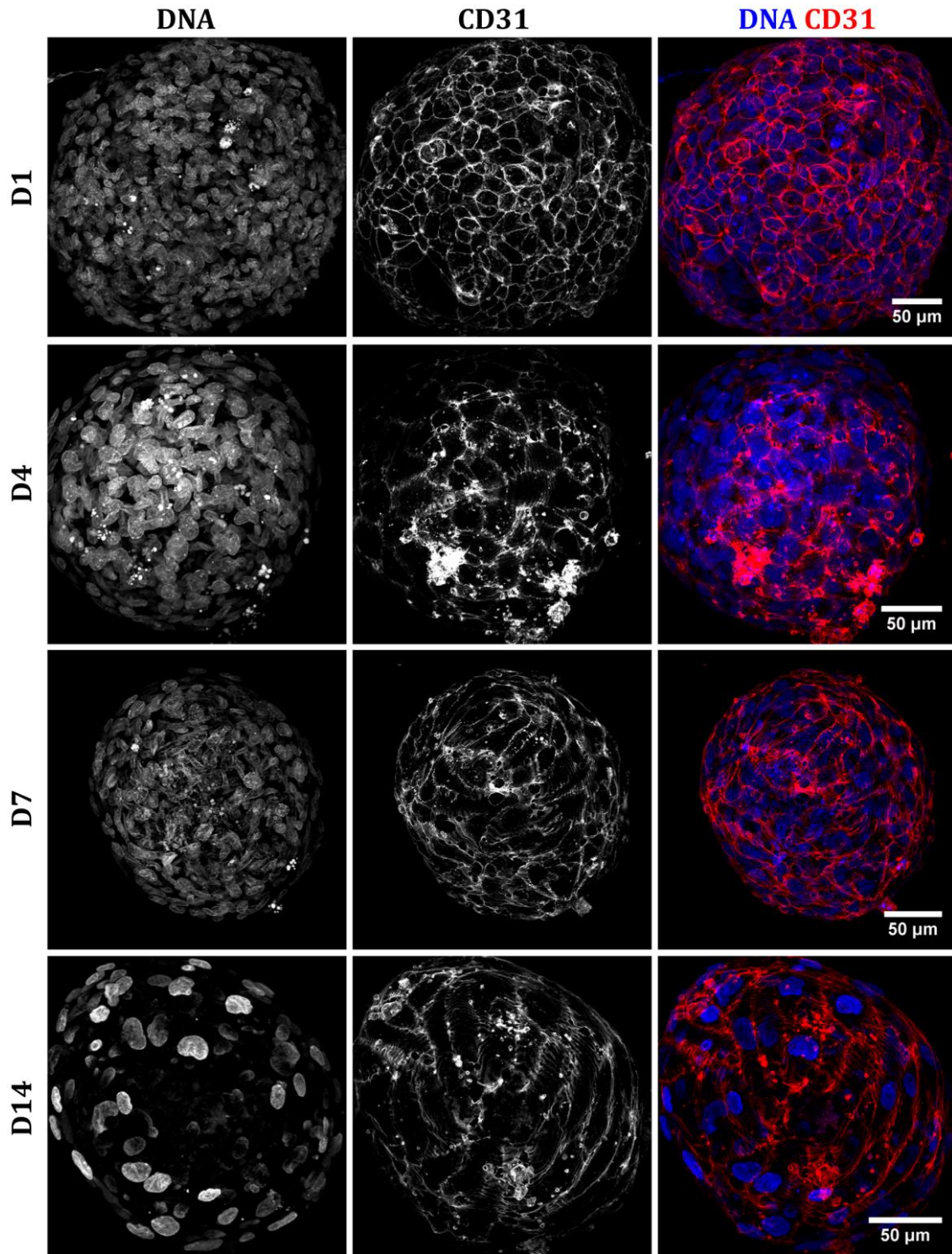
Figure 15 – Endothelial organization at the periphery of coculture spheroids. Immunostaining of CD31 (red) and counterstained with DAPI (blue). No staining from inside planes was taken into consideration as no CD31 fluorescence signal was collected. It is noteworthy that, contrarily to the other time points, at day 14 only DAPI from the most outer layers were acquired. Confocal images obtained using a Z stack step of 1,5 µm. For day 1, 7 and 14 a 40x objective was used, while for day 4 was used a 63x objective. Highlights, 1.5x.

Next, by co-staining sections for the expression of CD31 and FN, the OEC surface monolayer was found to lay down on the FN fibers aligned in the outer layers of the spheroids, with both OEC flattening and FN deposition occurring concomitantly, suggesting that FN fibers might, in fact, be involved in OEC orientation at the periphery (**Fig.16D**). Finally, in order to determine whether the proliferative activity of OEC was affected along time, sections were co-stained for the expression of CD31 and Ki67. As observed for the total number of cells within spheroids, the amount of OEC proliferating significantly decreased ($P<0.001$) during the first 4 days of culture, after which it remained significantly unchanged until the end of the experiment (**Fig.16E**).

The data suggests that the OEC surface monolayer polarized apically with OEC apical membrane in contact with culture medium and its basal surface in contact with deposited FN. However, no expression of regulators of apical-basal polarity in epithelial and endothelial cells[107–110], such as aPKC (data not shown) and ZO-1 were detected (**Fig.16F**).
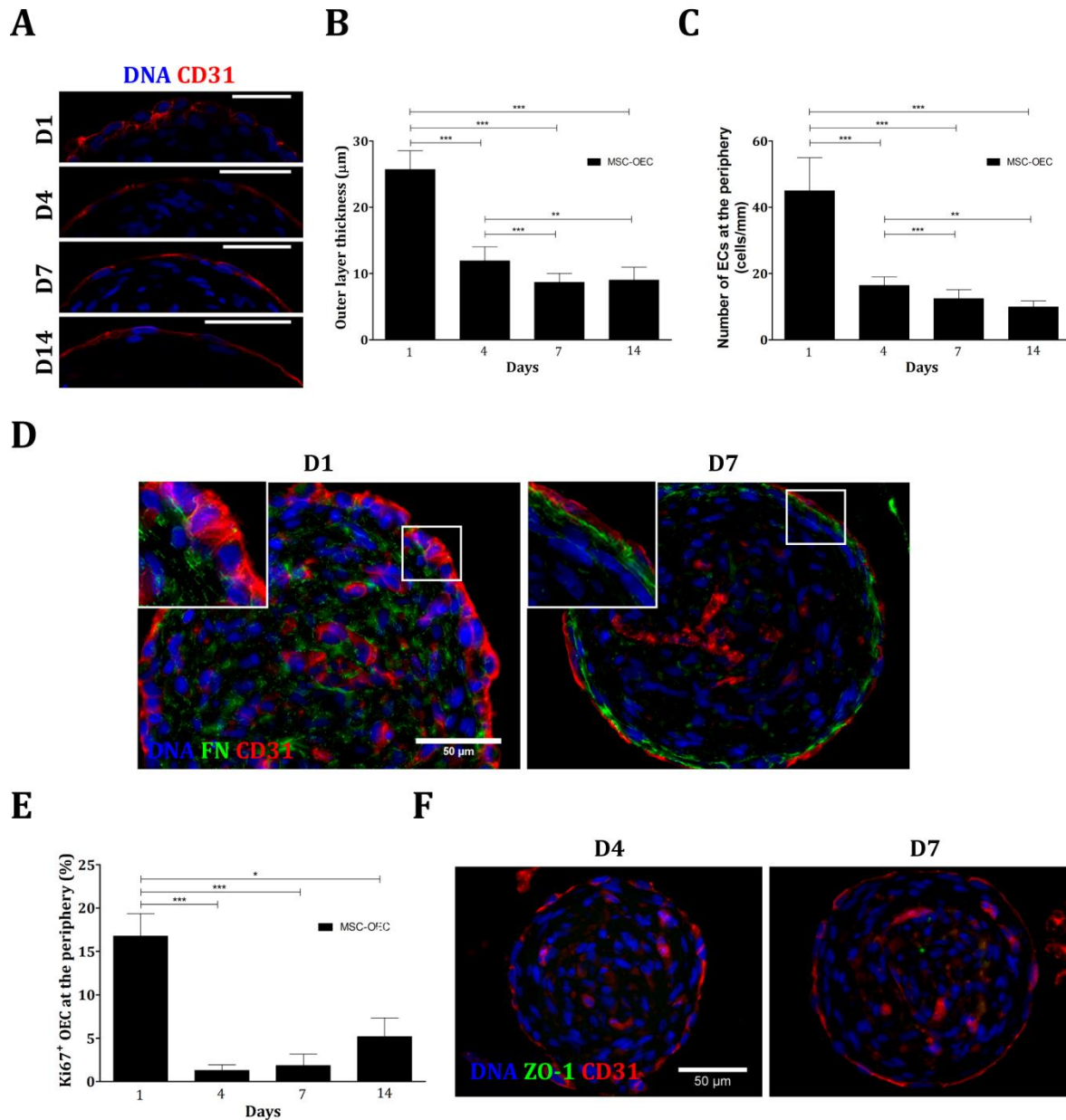
Figure 16 – Organization and phenotype of the OEC surface monolayer. (A) Confocal Z-planes illustrating the morphological changes in OEC at the periphery. Scale bar 50 μm; (B, C) Quantification of OEC flattening and the amount of OEC populating the surface monolayer, respectively, in sections stained against the expression of CD31. The thickness of the surface monolayer was determined as the average of, at least, 10 local measurements of OEC thickness, while the amount of OEC was detected by counting the number of CD31+ cells at the periphery and normalizing this number with the respective spheroid perimeter. Quantitative results are presented as mean ± SD (n=15, from 1 independent experiment), * p < 0.05, ** p < 0.001, *** p < 0.0001 student t-test for OEC flattening and Mann Whitney test for OEC at the periphery; (D) Co-staining of FN (green) and CD31(red) in coculture sections for day 4 and 7.; (E) Quantification OEC proliferative cells at the surface relatively to the total amount of OEC in that layer. Quantitative results are presented as mean ± SEM (n=10, from 1 independent experiment), * p < 0.05, ** p < 0.001, *** p < 0.0001, as determined by Mann Whitney test; (F) MSC-OEC spheroids sections stained for the expression of the apical-basal polarity regulator ZO-1 and against CD31 at day 4 and 7. No expression of ZO-1 was detected, particularly at the endothelial surface monolayer. Insets, 2x.

III.5.3. Endothelial clustering

As mentioned before, OEC formed some multicellular clusters at the more inner regions of the spheroids. Different assays suggested that cells within these clusters showed some signs of apoptosis. In H&E stainings, clusters appear as irregular structures with dark eosinophilic cytoplasm and purple nuclear chromatin fragments (**Fig.17A**), suggesting, respectively, cell shrinkage and nuclei fragmentation, two well-known processes of early apoptosis. Immunohistochemistry analysis also showed that these clusters were characterized by fragmented nuclei and a more diffuse CD31 expression rather than a typical membrane staining, as observed in isolated OEC (**Fig.17B**). Moreover, many clusters contained not only cells with fragmented nuclei and apparently apoptotic bodies (**Fig.17B-yellow arrow**), but also with chromatin condensation (**Fig.17B-green arrow**), suggesting that these clusters contain cells at different stages of programmed-cell death.

Although these data suggest an apoptotic phenotype, OEC clusters showed some degree of functionality. In fact, these structures were positive for other endothelial specific markers, including VE-Cadherin and vWF (**Fig.17C**). While vWF was confined to the intra space of OEC clusters, VE-cadherin was found surrounding OEC clusters. Furthermore, several OEC sproutings from these clusters were identified (**Fig.17D**), with an increasing number developing throughout culture (**Table 2**). To further assess if these OEC clusters were functional and even could guide the formation of neovessels-like structures, an additional experiment was performed, in which the end of culture was set to 21 days instead. By the end of the experiment, OEC clusters were still present inside the spheroids and with the same phenotype as previously described (**Fig.17E**).
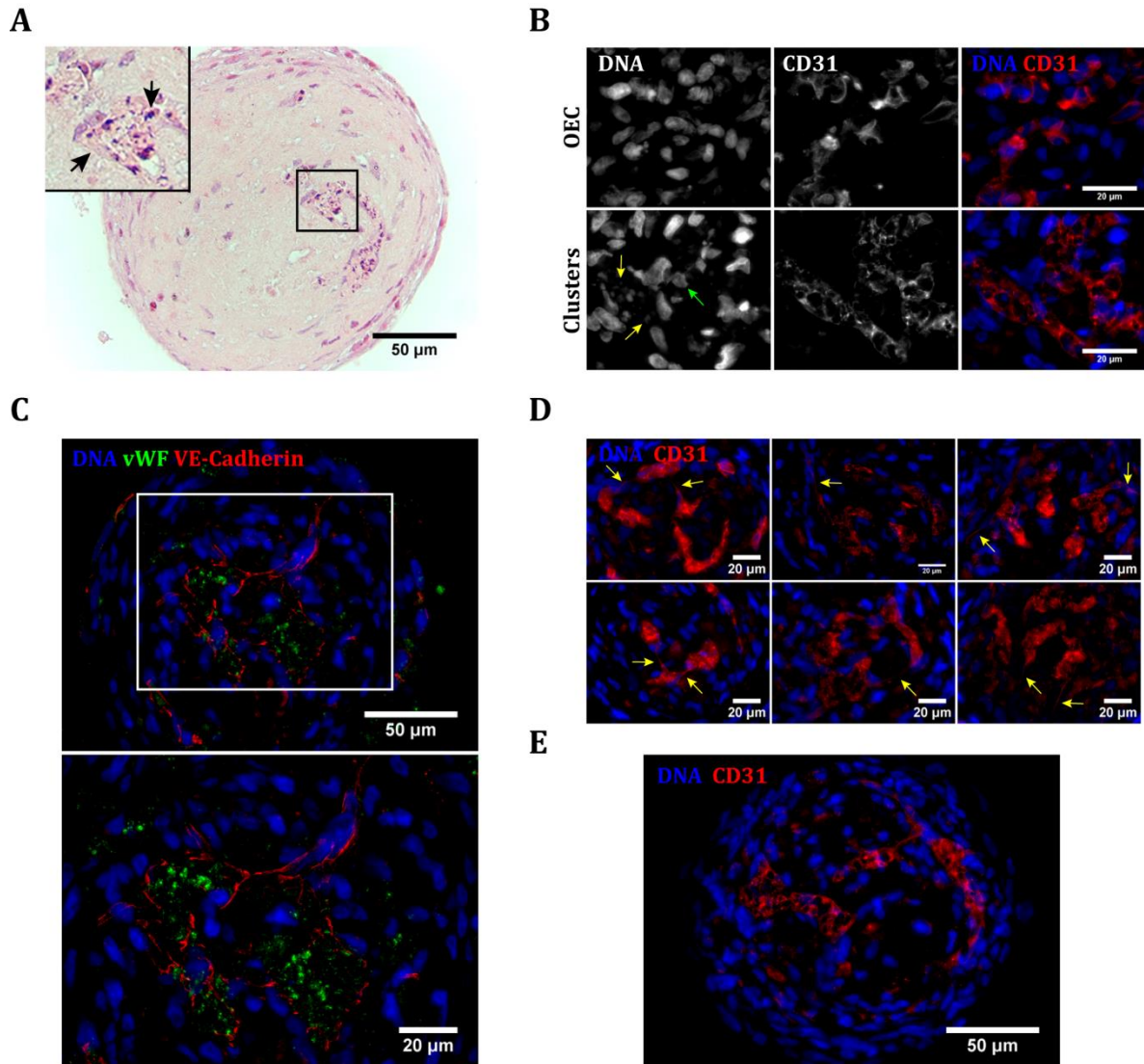
Figure 17 – OEC clustering within coculture spheroids. (A) H&E staining for MSC-OEC spheroids at day 14. OEC clusters were identified within spheroids as irregular structures with darker eosinophilic color and condensed chromatin (arrows). Inset, 2x; (B) OEC phenotype at day 1 (upper panel) and 14 (lower panel). Fragmented DNA was detected within clusters and CD31 signal was not so well-defined when comparing to isolated OEC. Scale bar 20 μm; (C) OEC clusters expression of vWF and VE-Cadherin at day 14; (D) Sproutings from OEC clusters (yellow arrows) in paraffin-embedded sections at day 7 and 14; (E) OEC clusters phenotype at day 21. Images were acquired using 40x (A-E) and 63x (highlight from C) magnifications.

Chapter IV

Discussion

Over the past years, some preclinical studies have been demonstrated that prevascularized spheroids can improve integration with the host's vasculature, ultimately leading to an enhanced cell engraftment. However, in general, little to no attention has been directed to their *in vitro* characterization in what concerns, for example, the type of vascular microstructures formed over time and ECM distribution. When spheroid transplantations proceed empirically without a deeper understanding of its complex bioengineered 3D cellular micromilieu, researchers may miss important biological outcomes. In this context, the present study aimed at developing and characterizing a prevascular spheroid system that could be potentially used for advanced CT in the future. Such study may contribute for a better understanding of endothelial patterning and maturation of vascular microstructures in coculture spheroids, providing important insights for CT. Herein, OEC were selected as the endothelial cell source, although the majority of the studies done so far used HUVEC instead. Despite inconsistencies among the scientific community about their definition and origin, OEC have been considered by some authors as "true EPC"[111,112]. Indeed, this cell type has been shown to contribute for neovessel formation by being recruited and integrated into pre-existing vessels[113] and/or by directly forming *de novo* vascular vessels[99,113]. Moreover, OEC are considered to be clinically more relevant than mature EC such as HUVEC, due to their higher expansion capacity in culture and to the easy accessibility from adult peripheral blood[111], constituting a potential source of autologous human EC. Umbilical cord blood, used herein, also represents a promising cell source for pro-angiogenic therapies[113].

The cell ratio is a well-known factor in vascular patterning within coculture spheroids, being highly dependent on the cell types. Since this topic is largely unexplored for OEC, in the present study, MSC were combined with OEC at a 1:1 cell ratio, as extensively adopted by studies previously conducted using HUVEC as the EC source[31,36,47,98,102,114]. It should be noted that, while this ratio has mostly induced organization of EC into concentric layers or endothelial cores[47,96,98,102,114], more recent studies reported that lower proportions of EC

favors the formation of primitive vascular-like networks[95,101]. However, no clear evidences have so far shown that vascular networks elicit a stronger angiogenic response *in vivo* than other vascular microstructures within engineered tissue constructs. In fact, a recent study reported that equal amounts of adipocyte-derived stem cells and EPC assembled into concentric spheroids, which, upon culture on Matrigel, revealed the strongest angiogenic response among spheroids with different vascular microstructures. Therefore, a 1:1 cell ratio remains a promising option for further studies.

To generate prevascularized spheroids, numerous studies have used different scaffold-free platforms, including pellets[59], nonadhesive culture dishes[65], microgravity modulators[62,63] and hanging-drops[28,35]. In general, researchers collect spheroids from the respective culture vessel and then ressuspend them in paraffin for further analysis. Herein, spheroids were not collected from the microwells but, instead, were directly embedded in paraffin, which resulted in a much higher number of spheroids per section. However, the maximum number of 81 units, the number of microwells per array used in this study, per section was not possible to obtain, mostly due to the loss of some spheroids during processing and discrepancies between the cutting angle and the microarray orientation, which were technically difficult to overcome. Nevertheless, this was the first time, according to the author's knowledge, that such approach using Microtissues' molds enabled a HT analysis of uniformed-size coculture spheroids.

In the present study, while MSC alone and combined with OEC assembled into compact spheroids inside nonadhesive microwells, OEC formed loose aggregates, which easily dissociated upon manipulation. In opposition to HUVEC[47,96,98] and human dermal microvascular endothelial cells (HDMEC)[115], which were found to assemble into compact spheroids, OEC have been previously demonstrated to form loose aggregates, when seeded in nonadhesive conditions[29]. Recent studies using 2D cultures have shown that OEC are not able to secrete ECM, particularly FN, collagen type IV and laminin, to the same extent as mature EC. Likewise, herein, by day 1, OEC aggregates did not secrete as much ECM as MSC alone or cocultures. As cell-ECM interactions are known to be critical for initial assembly and compaction of monodispersed cells[52], the low OEC potential to secrete ECM may, in part, impaired the extent of its compaction into spheroids. Furthermore, taking into consideration that in the presence of MSC, OEC were able to integrate into compact spheroids, these results suggest that MSC supported OEC throughout culture, in part, by secreting ECM, which probably enabled anchoring and survival of OEC.

Further morphological analysis was conducted by staining spheroids with H&E dyes. By day 4, both MSC and MSC-OEC spheroids were found to organize into heterogeneous tissue structures, with cells adopting a spindle-like shape at the periphery. This surface morphological polarization had been already reported both in MSC monocultures[116] and prevascularized spheroids[102]. According to current literature[117], aggregation of monodispersed cells into 3D spheroids leads to an increased cortical tension at the culture medium-spheroid interface that, in turn, induces a morphological adaptation of cells at the more external layers. Interestingly, by day 4, type IV collagen fibers were found to be aligned at the periphery of MSC and MSC-OEC spheroids that, most likely, was also due to the increased cortical tension. In this context, it would be interesting to analyze the mechanotransduction underlying the reported histological and ECM polarization.

Next, cell viability within spheroids was assessed by staining whole spheroids with standard live/dead dyes, but no fluorescence signal was possible to acquire in the innermost parts. This technical problem was observed for all time points and was probably related to the highly dense cellular structure, which might have impaired the diffusion of the fluorescent probes and/or enhanced the light scattering inside the spheroid, an optical effect well described in studies previously conducted in 3D spheroids[76,106].

Nevertheless, an initial decrease in metabolic activity followed by stabilization throughout culture was successfully detected using a resazurin assay, for both MSC and MSC-OEC spheroids. This initial decrease may, in part, be associated to an adaptation of MSC to the EC culture medium and/or to the transition of 2D precultured cells to a 3D cellular microenvironment. Yet, it should be noted that these cell metabolic values were not normalized by the total cell number per spheroid. Considering that, at least, for MSC-OEC spheroids, there was a significant cell loss after 4 days in culture, DNA quantification assays should be performed in order to make more reliable conclusions. Similarly, the cell proliferative activity within coculture spheroids also decreased during the first 4 days, which may be related to the aforementioned factors. It was also noted that, by day 4, cell proliferation was confined to the outer layers of the spheroids. Most likely, cells at the periphery had an easier access to nutrients and oxygen as compared to cells at the innermost areas. Although the assembled spheroids had a radius between 115 to 130 μm, which is within the limit of oxygen diffusion for spheroids (150 to 200 μm)[118], their highly dense cellular structure may have induced the creation of a hypoxic core. Indeed, an important complementary assay would be to determine whether a hypoxic core formed over time, by

staining against key regulators such as hypoxia-inducible factor (HIF)-1,2α. Hypoxic conditions not only interfere with cell activity within spheroids[119], but have also been demonstrated to guide the formation of vascular microstructures within prevascularized spheroids[28,93].

Despite the initial decrease in both metabolic activity and proliferation, cells remained active throughout culture and abundantly produced ECM components within spheroids, particularly collagen type IV and FN, both expected to augment cell retention and survival in the host tissue upon transplantation[36]. Indeed, MSC monocultures were found to express collagen type IV, but only after 4 days in culture, whereas in the presence of OEC, an extensive meshwork of type IV collagen fibers was detected since the onset of the experiment, suggesting that these cells play a role in dictating the pattern of ECM deposition. In addition, FN was present in MSC and MSC-OEC cultures for all the time points. Interestingly, while in MSC monocultures, FN was distributed throughout the whole spheroid, in cocultures, FN was confined to the outer layers as aligned fibers surrounding the tissue core. Collagen type IV, among other ECM components, constitutes the basement membrane of *in vivo* blood vessels and is a well-known regulator of neovessel formation and stabilization of vascular microstructures[120]. Also, FN is an ECM component of developing microvessels, playing a fundamental role in blood vessel morphogenesis during embryonic development and pathological neovessel formation[121]. However, few studies have addressed so far ECM expression and its role in vascular structure formation within coculture spheroids. One study demonstrated that coculture spheroids with homogeneously mixed MSC and HUVEC expressed FN, which was also randomly distributed within the spheroid[36]. Herein, OEC assembled into a surface monolayer, which flattened concomitantly to FN deposition at the periphery, ultimately forming an elongated endothelium supported on FN fibers. Although the origin of the secreted ECM components is not known, these results suggest that MSC and OEC in coculture spheroids established a bidirectional crosstalk, which accelerated the production of type IV collagen fibers and induced a polarization of FN fibers. However, further studies should be conducted in order to understand the true role of secreted ECM in OEC patterning and function.

One of the main goals was to study the formation and type of vascular microstructures within coculture spheroids, which could then be used for advanced CT. As shown here, OEC combined at equal amounts with MSC assembled within 24h into a continuous surface monolayer, which remained essentially intact until the end of the experiment. Similar vascular organization has already been reported using other EC types, mainly HUVEC. For instance, by

combining equal amounts of HUVEC and HUASMC in liquid methylcellulose, Korff and colleagues showed that, within 2 days, coculture spheroids spontaneously organized into a surface monolayer of EC, surrounding a core of HUASMC[98]. On the other hand, little to no attention has been directed to the study of spatial distribution of OEC in coculture spheroids. In a particular recent study, Hsu *et al.*[29] demonstrated that OEC were able to assemble into distinct vascular microstructures within coculture spheroids, including clusters and concentric layers, largely depending on the substrates where cells were cultured on, and cell ratio and type. As previously discussed in section I.6, over the past years, several studies have been demonstrating that vascular patterning in coculture spheroids is a complex dynamic process and regulated by numerous factors, which are far from being totally understood.

Herein, OEC were found to organize into essentially two types of microstructures. The majority of the OEC formed an external monolayer, adopting a flattened morphology, and the amount of proliferating OEC significantly decreased throughout culture, suggesting that OEC acquired an EC *in vivo*-like mature phenotype that closely mimics quiescent vasculature found in physiological tissues[98]. Although the presented data suggest that the OEC surface monolayer polarized apically with OEC apical membrane in contact with culture medium and its basal surfaces in contact with deposited ECM, particularly FN and type IV collagen fibers, staining for two well-known markers of apical-basal polarity was negative. Nevertheless, it should be noted that, although these markers were negatively tested both in paraffin-embedded and in frozen sections, no positive control was performed. Therefore, further studies should be performed to confirm whether OEC at the periphery effectively polarized over time.

In addition to the surface monolayer, some OEC remained entrapped inside the spheroids. Over time, the majority of these cells were lost as quantified by immunohistochemistry and flow cytometry analysis. Both approaches detected an increase of the cell ratio for day 1 and 4, whereas for day 7, flow cytometry determined a much lower value than immunohistochemical quantification. Such disparity might be explained by a technical problem occurred during flow analysis. Indeed, the exclusion of membrane-damaged cells by PI staining was performed in less time than needed. Taking into consideration that the OEC clusters, most likely apoptotic, emerged only by day 7, this technical problem might have overestimated the amount of OEC alive, especially for day 7. Previous studies, although using other cell types such as HUVEC and fibroblasts, also determined a similar significant loss of EC during the first week of coculture in spheroids[101]. According to the authors, EC attachment

and survival within spheroids critically depend on an optimal balance of heterologous interactions and thus an optimal cell ratio, which was reported to be ca. 10-to-1.

Over the last years, several studies have suggested that circulating EPC may, in fact, participate in adult neovessel formation during, for example, ischemic conditions[99,122]. However, the mechanisms by which EPC contribute for postnatal neovascularization are still a matter of debate[99]. One of the proposed mechanisms consists on a direct contribution, in which functional vessels are derived entirely from EPC. In a murine model of soft tissue ischemia, Tepper and colleagues[99] demonstrated that bone marrow-derived EPC were recruited to the lesion site, and after 7 days, formed proliferative clusters. By day 14, EPC clusters aligned and coalesced into vascular-like structures, which eventually became functional blood vessels by day 21.

In the present study, some OEC effectively formed clusters at the spheroids core, which appear reminiscent of those structures found *in vivo*. Moreover, some of these clusters showed some degree of endothelial sprouting overtime. In order to determine whether this clusters would follow a similar fate as found *in vivo*, ultimately forming a primitive vascular network, maturation was further assessed for up to 21 days in culture. Yet, while OEC clusters were still present within spheroids at that later time point, no capillary-like structures were detected. Apart from the expression of different EC-specific molecules and formation of sproutings, OEC clusters, in fact, showed some signs of apoptosis, including cell shrinkage and DNA fragmentation. As observed in paraffin-embedded sections counterstained with DAPI, clusters were composed of cells apparently at different stages of apoptosis, suggesting that OEC clusters were apparently formed due to asynchronous entry of neighboring cells into programmed-cell death, a process designated bystander killing[123]. The apoptotic nature of these clusters should be further confirmed, for example, by a Terminal deoxynucleotidyl transferase dUTP nick end labelin (TUNEL) assay and by staining sections against expression of 3-cleaved caspase.

Chapter V

Conclusion remarks and future perspectives

Over the past years, several preclinical studies have demonstrated that cells preassembled into spheroids can enhance cell delivery and long-term engraftment in the host's system, when compared to conventional single-cell approaches. Yet, while spheroids and particularly prevascularized ones show promise as a cell-based therapeutic approaches, their widely adoption has not been as fast as expected[26]. Indeed, the complex bioengineered vascular micromilieu created in prevascularized spheroids remains largely unexplored, which might hamper new insights for optimized treatments. The global acceptance of prevascularized spheroids will also depend on the development of platforms that enable not only production of large amounts of uniform spheroids, but also standard analysis in a HT manner.

In this context, the present study aimed at (1) developing, in a HT way, well-characterized prevascularized spheroids that could potentially be used as optimal cell-based therapeutics in the future; and (2) deciphering their 3D micromilieu with special focus on the formation of vascular microstructures and ECM deposition. For this purpose, cells were seeded on nonadhesive microwell arrays casted from precision molds, which within 24h, allowed the generation of 81 spheroids units per mold. Additionally, a new protocol was herein designed to process these spheroids directly inside the microwells, ultimately enabling simultaneous analysis of several spheroids per section. Thus, it was possible to scale up the production of spheroids, while at the same time perform a HT analysis. In fact, according to the author's knowledge, this was the first time that the commercially available molds enabled histological and immunohistochemical analysis in a HT way.

To generate prevascularized spheroids, numerous studies have been performed using mainly HUVEC as the EC source. In general, these cells revealed to be capable of forming different types of vascular microstructures within coculture spheroids, some of which were apparently

functional, increasing the angiogenic response upon transplantation in animal models. However, HUVEC do not constitute a clinically relevant EC source. In contrast, progenitor EC such as OEC exhibit a higher expansion capacity in culture and are easily obtained both from adult and neonatal sources, constituting an attractive, yet largely unexplored, EC type for the generation of prevascularized spheroids. Indeed, whether OEC are effectively capable of forming spheroids and vascular microstructures within them remains poorly understood.

In the present study, OEC were combined with MSC at a 1:1 cell ratio and cultured for up to 21 days. It was demonstrated that OEC, when in the presence of MSC, are capable of forming coculture spheroids exhibiting some key features that might be essential for successful cell engraftment upon transplantation. Indeed, OEC cocultured with MSC are able to form compact spheroids that maintained their integrity for long-term periods. Cells on these coculture spheroids were active and produced abundant amounts of ECM fibers, a well-known key requisite for improved cell retention and survival at the lesion site. Moreover, similarly to what was previously described for HUVEC, under the experimental conditions used herein, OEC are capable of assembling into specific vascular microstructures, particularly as an aligned monolayer at the spheroids surface and as clusters at the core. In future studies, it will be important to unveil the exact mechanisms driving such re-arrangements and their respective angiogenic potential when implanted *in vivo*.

From a fundamental perspective, it should also be noted that, over time, ECM polarized within spheroids only when OEC and MSC were both present in culture. Moreover, this polarization occurred concomitantly with OEC flattening at the surface. Thus, it seems that OEC and MSC established a bidirectional crosstalk, which modulated both cell phenotype and the microenvironment surrounding them. Yet, it should be noted that this comparison is based on data obtained from only one MSC monoculture experiment, and so, for validating this hypothesis, more biological replicates must be tested in future work. Nevertheless, data obtained in this study proved that OEC in the presence of MSC were capable of forming a dynamic and complex microenvironment, in which the maturation stage of cells and their microenvironment evolves over time. Whether prevascularized spheroids at different stages of maturation might lead to distinct angiogenic/neovascularization responses when implanted *in vivo* in adequate animal models remains to be studied. As preliminary screening tests, it would be interesting to transfer coculture spheroids at different maturation stages into Matrigel for assessing their angiogenic potential *in vitro*, and later using the CAM assay in order to determine the influence of maturation time on *in vivo* angiogenesis.

In conclusion, the present work enabled the production and analysis of pre-vascularized spheroids in a high throughput manner, and provided new insights regarding ECM and OEC patterning in coculture spheroids, that may contribute for future developments in spheroid-based CT.

References

1. Daley, G. Q. The promise and perils of stem cell therapeutics. *Cell Stem Cell* **10,** 740–749 (2012).

2. Fischbach, M. a, Bluestone, J. a & Lim, W. a. Cell-based therapeutics: the next pillar of medicine. *Sci. Transl. Med.* **5,** 179ps7 (2013).

3. Kelm, J. M. & Fussenegger, M. Scaffold-free cell delivery for use in regenerative medicine☆. *Adv. Drug Deliv. Rev.* **62,** 753–764 (2010).

4. Heathman, T. R. J. *et al.* The Translation of Cell-Based Therapies: Clinical Landscape and Manufacturing Challenges. *Regen. Med.* **10,** 49–64 (2015).

5. Passweg, J. R. *et al.* Hematopoietic stem cell transplantation: A review and recommendations for follow-up care for the general practitioner. *Swiss Med. Wkly.* **142,** 1–15 (2012).

6. Kemp, P. History of regenerative medicine: looking backwards to move forwards. *Regen. Med.* **1,** 653–669 (2006).

7. Mason, C. & Manzotti, E. Regenerative medicine cell therapies: numbers of units manufactured and patients treated between 1988 and 2010. *Regen. Med.* **5,** 307–313 (2010).

8. Trounson, A. & McDonald, C. Stem Cell Therapies in Clinical Trials: Progress and Challenges. *Cell Stem Cell* **17,** 11–22 (2015).

9. Barbash, I. M. *et al.* Systemic delivery of bone marrow-derived mesenchymal stem cells to the infarcted myocardium: Feasibility, cell migration, and body distribution. *Circulation* **108,** 863–868 (2003).

10. Dow, J., Simkhovich, B. Z., Kedes, L. & Kloner, R. a. Washout of transplanted cells from the heart: A potential new hurdle for cell transplantation therapy. *Cardiovasc. Res.* **67,** 301–307 (2005).

11. Penicka, M., Widimsky, P., Kobylka, P., Kozak, T. & Lang, O. Early Tissue Distribution of Bone Marrow Mononuclear Cells After Transcoronary Transplantation in a Patient With Acute Myocardial Infarction. *Circ.* **112 ,** e63–e65 (2005).

12. Cheng, K. *et al.* Magnetic targeting enhances engraftment and functional benefit of iron-labeled cardiosphere-derived cells in myocardial infarction. *Circ. Res.* **106,** 1570–1581 (2010).

13. Suzuki, K. *et al.* Role of interleukin-1?? in acute inflammation and graft death after cell transplantation to the heart. *Circulation* **110,** 219–225 (2004).

14. Freyman, T. *et al.* A quantitative, randomized study evaluating three methods of mesenchymal stem cell delivery following myocardial infarction. *Eur. Heart J.* **27,** 1114–1122 (2006).

15. Behfar, A., Crespo-Diaz, R., Terzic, A. & Gersh, B. J. Cell therapy for cardiac repair--lessons from clinical trials. *Nat. Rev. Cardiol.* **11,** 232–46 (2014).

16. Menasche, P. Cell-based therapy for heart disease: a clinically oriented perspective. *Mol. Ther.* **17,** 758–766 (2009).

17. Newland, B. *et al.* Tackling Cell Transplantation Anoikis: An Injectable, Shape Memory Cryogel Microcarrier Platform Material for Stem Cell and Neuronal Cell Growth. *Small* **11,** 5047–5053 (2015).

18. Jolla, L. & Jolla, L. Disruption of Epithelial Cell-Matrix Interactions Induces Apoptosis. **124,** 619–626 (1994).

19. Samper, E., Diez-Juan, a., Montero, J. a. & Sepúlveda, P. Cardiac Cell Therapy: Boosting Mesenchymal Stem Cells Effects. *Stem Cell Rev. Reports* 266–280 (2012). doi:10.1007/s12015-012-9353-z

20. Niagara, M. I., Haider, H. K., Jiang, S. & Ashraf, M. Pharmacologically preconditioned skeletal myoblasts are resistant to oxidative stress and promote angiomyogenesis via release of paracrine factors in the infarcted heart. *Circ. Res.* **100,** 545–555 (2007).

21. Huang, J. *et al.* Genetic modification of mesenchymal stem cells overexpressing ccr1 increases cell viability, migration, engraftment, and capillary density in the injured myocardium. *Circ. Res.* **106,** 1753–1762 (2010).

22. Lim, S. Y. *et al.* The effects of mesenchymal stem cells transduced with Akt in a porcine myocardial infarction model. *Cardiovasc. Res.* **70,** 530–542 (2006).

23. Martin, I. *et al.* The Survey on Cellular and Engineered Tissue Therapies in Europe in 2013. *Tissue Eng. - Part A* **22,** 5–16 (2016).

24. Cheng, A. Y. & García, A. J. Engineering the matrix microenvironment for cell delivery and engraftment for tissue repair. *Curr Opin Biotechnol.* **24,**864-871 (2013).

50

25. Silva, E. a, Kim, E.-S., Kong, H. J. & Mooney, D. J. Material-based deployment enhances efficacy of endothelial progenitor cells. *Proc. Natl. Acad. Sci. U. S. A.* **105,** 14347–52 (2008).

26. Comley, J. *Progress made in applying 3D cell culture technologies*. (2013).

27. Achilli, T.-M., Meyer, J. & Morgan, J. R. Advances in the formation, use and understanding of multi-cellular spheroids. *Expert Opin. Biol. Ther.* **12,** 1347–1360 (2012).

28. Kelm, J. M. *et al.* VEGF profiling and angiogenesis in human microtissues. *J. Biotechnol.* **118,** 213–229 (2005).

29. Hsu, S. *et al.* Substrate-dependent modulation of 3D spheroid morphology self-assembled in mesenchymal stem cell-endothelial progenitor cell coculture. *Biomaterials* **35,** 7295–7307 (2014).

30. Dissanayaka, W. L., Zhu, L., Hargreaves, K. M., Jin, L. & Zhang, C. In Vitro Analysis of Scaffold-free Prevascularized Microtissue Spheroids Containing Human Dental Pulp Cells and Endothelial Cells. *J. Endod.* **41,** 663–670 (2015).

31. Dissanayaka, W. L., Zhu, L., Hargreaves, K. M., Jin, L. & Zhang, C. Scaffold-free Prevascularized Microtissue Spheroids for Pulp Regeneration. *J. Dent. Res.* **93,** 1296–303 (2014).

32. Hirschhaeuser, F. *et al.* Multicellular tumor spheroids: An underestimated tool is catching up again. *J. Biotechnol.* **148,** 3–15 (2010).

33. Gevensleben, H. *et al.* Comparison of MammaPrint and TargetPrint results with clinical parameters in German patients with early stage breast cancer. *Int. J. Mol. Med.* **26,** 837–843 (2010).

34. Meissner, K. K., Kirkham, D. L. & Doering, L. C. Transplants of neurosphere cell suspensions from aged mice are functional in the mouse model of Parkinson's. *Brain Res.* **1057,** 105–112 (2005).

35. Kelm, J. M. & Fussenegger, M. Microscale tissue engineering using gravity-enforced cell assembly. *Trends Biotechnol.* **22,** 195–202 (2004).

36. Chen, D.-Y. *et al.* Three-dimensional cell aggregates composed of HUVECs and cbMSCs for therapeutic neovascularization in a mouse model of hindlimb ischemia. *Biomaterials* **34,** 1995–2004 (2013).

37. Frith, J. E., Thomson, B. & Genever, P. G. Dynamic three-dimensional culture methods enhance mesenchymal stem cell properties and increase therapeutic potential. *Tissue Eng. Part C Methods* **16,** 735–749 (2009).

38. Bartosh, T. J. *et al.* Aggregation of human mesenchymal stromal cells (MSCs) into 3D spheroids enhances their antiin fl ammatory properties. *Proc. Natl. Acad. Sci. U. S. A.* **107,** 13724–13729 (2010).

39. Zhao, X. *et al.* Three-Dimensional Aggregates Enhance the Therapeutic Effects of Adipose Mesenchymal Stem Cells for Ischemia-Reperfusion Induced Kidney Injury in Rats. (2015).

40. Kelm, J. M. *et al.* A novel concept for scaffold-free vessel tissue engineering: Self-assembly of microtissue building blocks. *J. Biotechnol.* **148,** 46–55 (2010).

41. Emmert, M. Y., Hitchcock, R. W. & Hoerstrup, S. P. Cell therapy, 3D culture systems and tissue engineering for cardiac regeneration. *Adv. Drug Deliv. Rev.* **69-70,** 254–269 (2014).

42. Vegas, A. J. *et al.* Long-term glycemic control using polymer-encapsulated human stem cell–derived beta cells in immune-competent mice. *Nat. Med.* (2016). doi:10.1038/nm.4030

43. Simpson, D., Liu, H., Fan, T.-H. M., Nerem, R. & Dudley, S. C. A tissue engineering approach to progenitor cell delivery results in significant cell engraftment and improved myocardial remodeling. *Stem Cells* **25,** 2350–7 (2007).

44. Le Visage, C. *et al.* Mesenchymal stem cell delivery into rat infarcted myocardium using a porous polysaccharide-based scaffold: a quantitative comparison with endocardial injection. *Tissue Eng. Part A* **18,** 35–44 (2012).

45. Foty, R. a. & Steinberg, M. S. The differential adhesion hypothesis: a direct evaluation. *Dev. Biol.* **278,** 255–263 (2005).

46. Steinberg, M. S. Mechanism of tissue reconstruction by dissociated cells. II. Time-course of events. *Science* **137,** 762–763 (1962).

47. Dean, D. M., Napolitano, a. P., Youssef, J. & Morgan, J. R. Rods, tori, and honeycombs: the directed self-assembly of microtissues with prescribed microscale geometries. *FASEB J.* **21,** 4005–4012 (2007).

48. Rago, A. P., Dean, D. M. & Morgan, J. R. Controlling cell position in complex heterotypic 3D microtissues by tissue fusion. *Biotechnol. Bioeng.* **102,** 1231–1241 (2009).

49. Lin, R. Z., Chou, L. F., Chien, C. C. M. & Chang, H. Y. Dynamic analysis of hepatoma spheroid formation: Roles of E-cadherin and ??1-integrin. *Cell Tissue Res.* **324,** 411–422 (2006).

50. Duguay, D., Foty, R. a. & Steinberg, M. S. Cadherin-mediated cell adhesion and tissue segregation: Qualitative and quantitative determinants. *Dev. Biol.* **253,** 309–323 (2003).

51. Shimazui, T. *et al.* Role of complex cadherins in cell-cell adhesion evaluated by spheroid formation in renal cell carcinoma cell lines. *Oncol. Rep.* **11,** 357–360 (2004).

52. Robinson, E. E., Zazzali, K. M., Corbett, S. & Foty, R. Alpha5beta1 integrin mediates strong tissue cohesion. *J. Cell Sci.* **116,** 377–386 (2003).

53. Casey, R. C. *et al.* Beta 1-integrins regulate the formation and adhesion of ovarian carcinoma multicellular spheroids. *Am. J. Pathol.* **159,** 2071–80 (2001).

54. Salmenperä, P. *et al.* Formation and activation of fibroblast spheroids depend on fibronectin–integrin interaction. *Exp. Cell Res.* **314,** 3444–3452 (2008).

55. Halbleib, J. M. & Nelson, W. J. Cadherins in development: Cell adhesion, sorting, and tissue morphogenesis. *Genes Dev.* **20,** 3199–3214 (2006).

56. Foty, R. a. & Steinberg, M. S. Cadherin-mediated cell-cell adhesion and tissue segregation in relation to malignancy. *Int. J. Dev. Biol.* **48,** 397–409 (2004).

57. Napolitano, A. P., Chai, P., Dean, D. M. & Morgan, J. R. Dynamics of the Self-Assembly of Complex Cellular Aggregates on Micromolded Nonadhesive Hydrogels. *Tissue Eng.* **13,** 2087–2094 (2007).

58. Bao, B., Jiang, J., Yanase, T., Nishi, Y. & Morgan, J. R. Connexon-mediated cell adhesion drives microtissue self-assembly. *FASEB J.* **25,** 255–264 (2011).

59. Jähn, K., Richards, R. G., Archer, C. W. & Stoddart, M. J. Pellet culture model for human primary osteoblasts. *Eur. Cell. Mater.* **20,** 149–161 (2010).

60. Han, Y. *et al.* Cultivation of recombinant Chinese hamster ovary cells grown as suspended aggregates in stirred vessels. *J. Biosci. Bioeng.* **102,** 430–435 (2006).

61. Brophy, C. M. *et al.* Rat hepatocyte spheroids formed by rocked technique maintain differentiated hepatocyte gene expression and function. *Hepatology* **49,** 578–586 (2009).

62. Becker, J. L. & Souza, G. R. Using space-based investigations to inform cancer research on Earth. *Nat. Rev. Cancer* **13,** 315–327 (2013).

63. Grimm, D. *et al.* Growing Tissues in Real and Simulated Microgravity: New Methods for Tissue Engineering. *Tissue Eng. Part B Rev.* **20,** 555–566 (2014).

64. Li, Q. *et al.* 3D Models of Epithelial-Mesenchymal Transition in Breast Cancer Metastasis: High-Throughput Screening Assay Development, Validation, and Pilot Screen. *J. Biomol. Screen.* **16,** 141–154 (2011).

65. Vantangoli, M. M., Madnick, S. J., Huse, S. M., Weston, P. & Boekelheide, K. MCF-7 Human Breast Cancer Cells Form Differentiated Microtissues in Scaffold-Free Hydrogels. *PLoS One* **10,** e0135426 (2015).

66. Kelm, J. M. *et al.* Design of custom-shaped vascularized tissues using microtissue spheroids as minimal building units. *Tissue Eng.* **12,** 2151–2160 (2006).

67. Denker, A. E., Nicoll, S. B. & Tuan, R. S. of murine C3HlOTU2 cells upon treatment with transforming growth factor-pl. 25–34 (1995).

68. Souza, G. R. *et al.* Three-dimensional tissue culture based on magnetic cell levitation. *Nat. Nanotechnol.* **5,** 291–6 (2010).

69. Chan, H. F. *et al.* Rapid formation of multicellular spheroids in double-emulsion droplets with controllable microenvironment. *Sci. Rep.* **3,** 1–8 (2013).

70. Vadivelu, R. K. *et al.* Generation of three-dimensional multiple spheroid model of olfactory ensheathing cells using floating liquid marbles. *Sci. Rep.* **5,** 15083 (2015).

71. Kim, J. Bin. Three-dimensional tissue culture models in cancer biology. *Semin. Cancer Biol.* **15,** 365–377 (2005).

72. Breslin, S. & O'Driscoll, L. Three-dimensional cell culture: The missing link in drug discovery. *Drug Discov. Today* **18,** 240–249 (2013).

73. Ivascu, A. & Kubbies, M. Rapid Generation of Single-Tumor Spheroids for High-Throughput Cell Function and Toxicity Analysis. *J. Biomol. Screen.* **11,** 922–932 (2006).

74. Sakai, Y., Yamagami, S. & Nakazawa, K. Comparative analysis of gene expression in rat liver tissue and monolayer- and spheroid-cultured hepatocytes. *Cells Tissues Organs* **191,** 281–288 (2010).

75. Drinking, A. O. F. A better brew. *New Yorker,* 1–12 (2008). doi:http://dx.doi.org/Article

76. Dingle, Y.-T. L. *et al.* 3D Neural Spheroid Culture: An In Vitro Model for Cortical Studies. *Tissue Eng. Part C Methods* 1–39 (2015).

77. Lee, G. H., Lee, J. S., Wang, X. & Hoon Lee, S. Bottom-Up Engineering of Well-Defined 3D Microtissues Using Microplatforms and Biomedical Applications. *Adv. Healthc. Mater.* n/a–n/a (2015). doi:10.1002/adhm.201500107

78. Kwapiszewska, K., Michalczuk, a, Rybka, M., Kwapiszewski, R. & Brzózka, Z. A microfluidic-based platform for tumour spheroid culture, monitoring and drug screening. *Lab Chip* **14,** 2096–104 (2014).

79. Tung, Y.-C. *et al.* High-throughput 3D spheroid culture and drug testing using a 384 hanging drop array. *Analyst* **136,** 473–478 (2011).

80. Raghavan, S., Ward, M. R., Katelyn R Rowleyb, R. M. W. S. T. & Mehta, G. Formation of stable small cell number three-dimensional ovarian cancer spheroids using hanging drop arrays for preclinical drug sensitivity assays. *Gynecol. Oncol.* **138,** 181–189 (2015).

81. Jaganathan, H. *et al.* Three-Dimensional In Vitro Co-Culture Model of Breast Tumor using Magnetic Levitation. *Sci. Rep.* **4,** 6468 (2014).

82. Tseng, H. *et al.* A spheroid toxicity assay using magnetic 3D bioprinting and real-time mobile device-based imaging. *Sci. Rep.* **5,** 13987 (2015).

83. Haisler, W. L. *et al.* Three-dimensional cell culturing by magnetic levitation. *Nat. Protoc.* **8,** 1940–1949 (2013).

84. Timm, D. M. *et al.* A high-throughput three-dimensional cell migration assay for toxicity screening with mobile device-based macroscopic image analysis. *Sci. Rep.* **3,** 1–8 (2013).

85. Brouzes, E. *et al.* Droplet microfluidic technology for single-cell high-throughput screening. *Proc. Natl. Acad. Sci. U. S. A.* **106,** 14195–200 (2009).

86. McMillan, K. S., McCluskey, A. G., Sorensen, A., Boyd, M. & Zagnoni, M. Emulsion technologies for multicellular tumour spheroid radiation assays. *Analyst* **141,** 100–110 (2015).

87. Rakszewska, A., Tel, J., Chokkalingam, V. & Huck, W. T. One drop at a time: toward droplet microfluidics as a versatile tool for single-cell analysis. *NPG Asia Mater.* **6,** e133 (2014).

88. Tremblay, P. L., Hudon, V., Berthod, F., Germain, L. & Auger, F. a. Inosculation of tissue-engineered capillaries with the host's vasculature in a reconstructed skin transplanted on mice. *Am. J. Transplant.* **5,** 1002–1010 (2005).

89. Laschke, M. W. & Menger, M. D. Prevascularization in tissue engineering: Current concepts and future directions. *Biotechnol. Adv.* **34,** 112–121 (2015).

90. Rouwkema, J. & Khademhosseini, A. Vascularization and Angiogenesis in Tissue Engineering: Beyond Creating Static Networks. *Trends Biotechnol.* **xx,** 1–13 (2016).

91. Rouwkema, J., Rivron, N. C. & van Blitterswijk, C. a. Vascularization in tissue engineering. *Trends Biotechnol.* **26,** 434–441 (2008).

92. Levenberg, S. *et al.* Engineering vascularized skeletal muscle tissue. *Nat Biotechnol* **23,** 879–884 (2005).

93. Kelm, J. M. *et al.* Design of custom-shaped vascularized tissues using microtissue spheroids as minimal building units. *Tissue Eng.* **12,** 2151–2160 (2006).

94. Verseijden, F. *et al.* Prevascular structures promote vascularization in engineered human adipose tissue constructs upon implantation. *Cell Transplant.* **19,** 1007–1020 (2010).

95. Rouwkema, J., de Boer, J. & Van Blitterswijk, C. a. Endothelial cells assemble into a 3-dimensional prevascular network in a bone tissue engineering construct. *Tissue Eng.* **12,** 2685–2693 (2006).

96. Stahl, A. *et al.* Bi-directional cell contact-dependent regulation of gene expression between endothelial cells and osteoblasts in a three-dimensional spheroidal coculture model. *Biochem. Biophys. Res. Commun.* **322,** 684–692 (2004).

97. Noguchi, R. *et al.* Development of a three-dimensional pre-vascularized scaffold-free contractile cardiac patch for treating heart disease. *J. Hear. Lung Transplant.* **35,** 137–145 (2016).

98. Korff, T., Kimmina, S., Martiny-Baron, G. & Augustin, H. G. Blood vessel maturation in a 3-dimensional spheroidal coculture model: direct contact with smooth muscle cells regulates endothelial cell quiescence and abrogates VEGF responsiveness. *FASEB J.* **15,** 447–457 (2001).

99. Tepper, O. M. *et al.* Adult vasculogenesis occurs through in situ recruitment, proliferation, and tubulization of circulating bone marrow-derived cells. *Blood* **105,** 1068–1077 (2005).

100. Ribatti, D., Vacca, A., Nico, B., Roncali, L. & Dammacco, F. Postnatal vasculogenesis. *Mech. Dev.* **100,** 157–163 (2001).

101. Kunz-Schughart, L. a *et al.* Potential of fibroblasts to regulate the formation of three-dimensional vessel-like structures from endothelial cells in vitro. *Am. J. Physiol. Cell Physiol.* **290,** C1385–98 (2006).

102. Saleh, F. a, Whyte, M. & Genever, P. G. Effects of endothelial cells on human mesenchymal stem cell activity in a three-dimensional in vitro model. *Eur. Cell. Mater.* **22,** 242–57; discussion 257 (2011).

103. Williams, P. a. *et al.* Hypoxia augments outgrowth endothelial cell (OEC) sprouting and directed migration in response to sphingosine-1-phosphate (S1P). *PLoS One* **10,** 1–16 (2015).

104. LaBarbera, D. V, Reid, B. G. & Yoo, B. H. The multicellular tumor spheroid model for high-throughput cancer drug discovery. *Expert Opin. Drug Discov.* **7,** 819–830 (2012).

105. Hadjizadeh, A. & Doillon, C. J. Directional migration of endothelial cells towards angiogenesis using polymer fibres in a 3D co-culture system. *J. Tissue Eng. Regen. Med.* **4,** 524–531 (2010).

106. Kabadi, P. K. *et al.* Into the depths: Techniques for in vitro threedimensional microtissue visualization. *Biotechniques* **59,** 279–286 (2015).

107. Suzuki, A. & Ohno, S. The PAR-aPKC system: lessons in polarity. *J. Cell Sci.* **119,** 979–987 (2006).

108. Zovein, A. C. *et al.* ??1 Integrin Establishes Endothelial Cell Polarity and Arteriolar Lumen Formation via a Par3-Dependent Mechanism. *Dev. Cell* **18,** 39–51 (2010).

109. Cereijido, M., Contreras, R. G., Shoshani, L., Flores-Benitez, D. & Larre, I. Tight junction and polarity interaction in the transporting epithelial phenotype. *Biochim. Biophys. Acta - Biomembr.* **1778,** 770–793 (2008).

110. Tornavaca, O. *et al.* ZO-1 controls endothelial adherens junctions, cell-cell tension, angiogenesis, and barrier formation. *J. Cell Biol.* **208,** 821–838 (2015).

111. Costa-Almeida, R. *et al.* Fibroblast-Endothelial Partners for Vascularization Strategies in Tissue Engineering. *Tissue Eng. Part A* **00,** 1–11 (2014).

112. Medina, R. J. *et al.* Molecular analysis of endothelial progenitor cell (EPC) subtypes reveals two distinct cell populations with different identities. *BMC Med Genomics* **3,** 18 (2010).

113. Yoder, M. C. Human endothelial progenitor cells. *Cold Spring Harb. Perspect. Med.* **2,** 1–14 (2012).

114. Wenger, A. *et al.* Development and characterization of a spheroidal coculture model of endothelial cells and fibroblasts for improving angiogenesis in tissue engineering. *Cells. Tissues. Organs* **181,** 80–8 (2005).

115. Walser, R. *et al.* Generation of co-culture spheroids as vascularisation units for bone tissue engineering. *Eur. Cells Mater.* **26,** 222–233 (2013).

116. Yu, G. *et al.* Page 1 of 42 1. *J. Neurotrauma* 1–42 (2015). doi:DOI: 10.1089/ars.2010.3491

117. Sart, S., Tsai, A.-C., Li, Y. & Ma, T. Three-dimensional aggregates of mesenchymal stem cells: cellular mechanisms, biological properties, and applications. *Tissue Eng. Part B. Rev.* **20,** 365–80 (2014).

118. Nichols, M. G. & Foster, T. H. Oxygen diffusion and reaction kinetics in the photodynamic therapy of multicell tumour spheroids. *Phys. Med. Biol.* **39,** 2161–2181 (1994).

119. Asthana, A. & Kisaalita, W. S. Microtissue size and hypoxia in HTS with 3D cultures. *Drug Discov. Today* **17,** 810–817 (2012).

120. Daley, W. P., Peters, S. B. & Larsen, M. Extracellular matrix dynamics in development and regenerative medicine. *J. Cell Sci.* **121,** 255–264 (2008).

121. Van Obberghen-Schilling, E. *et al.* Fibronectin and tenascin-C: Accomplices in vascular morphogenesis during development and tumor growth. *Int. J. Dev. Biol.* **55,** 511–525 (2011).

122. Zhang, Z. G., Zhang, L., Jiang, Q. & Chopp, M. Bone marrow-derived endothelial progenitor cells participate in cerebral neovascularization after focal cerebral ischemia in the adult mouse. *Circ. Res.* **90,** 284–288 (2002).

123. Reznikov, K. *et al.* Clustering of apoptotic cells via bystander killing by peroxides. *FASEB J.* **14,** 1754–64 (2000).